DMD Fast Forward. Published on September 10, 2019 as DOI: 10.1124/dmd.119.086918
This article has not been copyedited and formatted. The final version may differ from this version.

DMD # 86918

Systematic Development and Verification of A Physiologically-Based Pharmacokinetic Model of Rivaroxaban

Eleanor Jing Yi Cheong[1], Denise Wun Xi Teo[1], Denise Xin Yi Chua[1] and Eric Chun Yong Chan[1,2]

[1]Department of Pharmacy, Faculty of Science, National University of Singapore, 18 Science Drive 4, Singapore 117543; [2]National University Cancer Institute, Singapore (NCIS), NUH Medical Centre (NUHMC), 5 Lower Kent Ridge Road, Singapore 119074

Note: Eleanor Jing Yi Cheong, Denise Wun Xi Teo and Denise Xin Yi Chua contributed equally to the manuscript.

DMD Fast Forward. Published on September 10, 2019 as DOI: 10.1124/dmd.119.086918
This article has not been copyedited and formatted. The final version may differ from this version.

Running title: PBPK Modeling of Rivaroxaban

Address correspondence to:

Professor Eric Chun Yong Chan, Department of Pharmacy, Faculty of Science, National University of Singapore, 18 Science Drive 4, Singapore 117543, Singapore.

Email: phaccye@nus.edu.sg; Telephone: 65-6516 6137; Fax: +65-67791554

Number of Text Pages	21
Number of Tables	6
Number of Figures	6
Number of References	54
Number of Words in the Abstract	246
Number of Words in the Introduction	687
Number of Words in the Discussion	1719

ABBREVIATIONS

AF	Atrial Fibrillation
AUC	Area under the plasma concentration-time curve
CL/F	Apparent clearance
CLu_{int}	Unbound intrinsic clearance
CL_{PD}	Passive diffusion clearance

CL_R	Renal clearance
CYP2J2	Cytochrome P450 2J2
CYP3A4	Cytochrome P450 3A4
C_{max}	Peak plasma concentration
DDI	Drug-Drug Interaction
DDDI	Drug-Drug-Disease Interaction
DOAC	Direct oral anticoagulant
USFDA	United States Food and Drug Administration
IVIVE	*In vitro* to *in vivo* extrapolation
J_{max}	Maximum rate of active transport
K_m	Michaelis constant
$K_{m:w}$	Bile micelle: water partition coefficient
K_p	Tissue: plasma partition coefficient
P_{app}	*In vitro* apparent permeability
PBPK	Physiologically-based pharmacokinetic
$P_{eff,man}$	Effective permeability in human
P-gp	P-glycoprotein
PTCPGK	Proximal tubular cells per gram kidney
S_0	Intrinsic Solubility

ABSTRACT

Rivaroxaban is indicated for stroke prevention in nonvalvular atrial fibrillation (AF). Its elimination is mediated by both hepatic metabolism and renal excretion. Consequently, its clearance is susceptible to both intrinsic (pathophysiological) and extrinsic (concomitant drugs) variabilities that in turn implicate bleeding risks. Upon systematic model verification, physiologically-based pharmacokinetic (PBPK) models are qualified for the quantitative rationalization of complex drug-drug-disease interactions (DDDIs). Hence, this study aimed to develop and verify a PBPK model of rivaroxaban systematically. Key parameters required to define rivaroxaban's disposition were either obtained from *in vivo* data or generated via *in vitro* metabolism and transport kinetic assays. Our developed PBPK model successfully predicted rivaroxaban's clinical PK parameters within predefined success metrics. Consideration of basolateral organic anion transporter 3 (OAT3)-mediated proximal tubular uptake in tandem with apical P-glycoprotein (P-gp)-mediated efflux facilitated mechanistic characterization of the renal elimination of rivaroxaban in both healthy and renal impaired patients. Retrospective drug-drug interaction (DDI) simulations, incorporating *in vitro* metabolic inhibitory parameters, accurately recapitulated clinically observed attenuation of rivaroxaban's hepatic clearance due to enzyme-mediated DDIs with CYP3A4/2J2 inhibitors (verapamil and ketoconazole). Notably, transporter-mediated DDI simulations between rivaroxaban and P-gp inhibitor ketoconazole yielded minimal increases in rivaroxaban's systemic exposure when P-gp-mediated efflux was solely inhibited but were successfully characterized when concomitant basolateral uptake inhibition was incorporated in the simulation. In conclusion, our developed PBPK model of rivaroxaban is systematically verified for prospective interrogation and management of untested yet clinically relevant DDDIs pertinent to AF management using rivaroxaban.

SIGNIFICANCE STATEMENT

Rivaroxaban is susceptible to drug-drug-disease interactions (DDDIs) comprising renal impairment, P-gp and CYP3A4/2J2 inhibition. Here, systematic construction and verification of a PBPK model of rivaroxaban, with the inclusion of a mechanistic kidney component, provided insight into the previously arcane role of OAT3-mediated basolateral uptake in influencing both clinically-observed renal elimination of rivaroxaban and differential extents of transporter-mediated DDIs. The verified model holds potential for investigating clinically-relevant DDDIs involving rivaroxaban and designing dosing adjustments to optimize its pharmacotherapy in atrial fibrillation.

DMD Fast Forward. Published on September 10, 2019 as DOI: 10.1124/dmd.119.086918
This article has not been copyedited and formatted. The final version may differ from this version.

VISUAL ABSTRACT

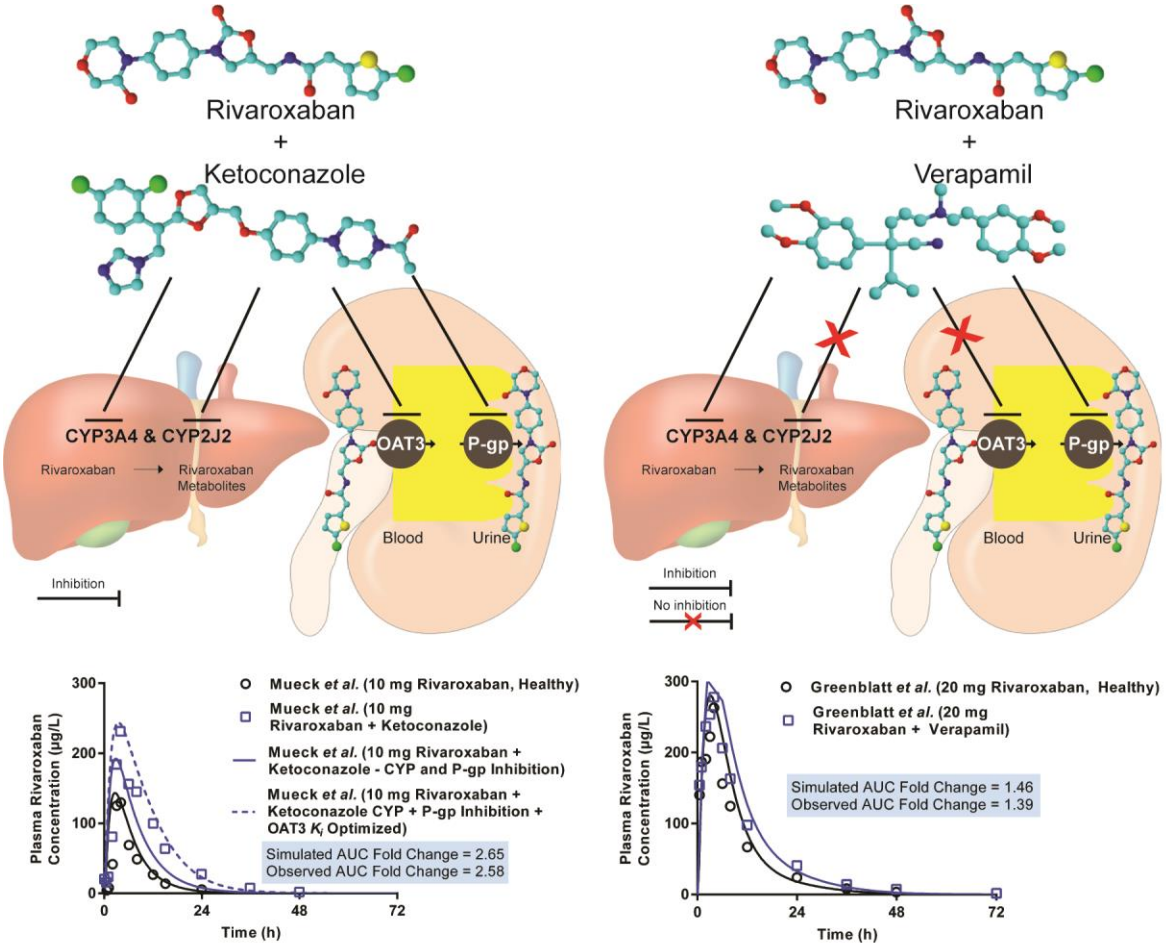

INTRODUCTION

Atrial fibrillation (AF) is the most common and clinically significant cardiovascular rhythm disorder. The Global Burden of Diseases, Injuries, and Risk Factors 2010 study indicated that the previous two decades have witnessed a progressive increase in the worldwide prevalence and incidence of AF, with significant effects on associated morbidity and mortality (Chugh *et al.*, 2014). Therapeutic mainstays of AF management can be chiefly divided into symptomatic treatment of arrhythmia by either rate or rhythm control, and prevention of thromboembolic complications by anticoagulation (January *et al.*, 2014).

In recent years, direct oral anticoagulants (DOACs) have emerged as preferred alternatives to warfarin, particularly due to predictable dose response relationships that eliminate the need for routine laboratory monitoring (Scaglione, 2013). Rivaroxaban, a non-vitamin K antagonist OAC approved by the United States Food and Drug Administration (USFDA) in 2010, is indicated for stroke prevention in nonvalvular AF. Rivaroxaban possesses a unique dual mode of elimination: where two thirds of the systematically absorbed dose undergo cytochrome P450 (CYP) 3A4/2J2-mediated metabolism while the remaining one third is excreted unchanged in the urine, primarily via P-glycoprotein (P-gp)-mediated efflux (Mueck *et al.*, 2013). This inevitably increases rivaroxaban's susceptibility to drug-drug-disease interactions (DDDIs) attributed to simultaneous impairment of its multiple clearance pathways (Grillo *et al.*, 2012).

The likelihood of drug-drug interactions (DDIs) is markedly increased when we consider that many rhythm and rate control agents (e.g. amiodarone, carvedilol and diltiazem) likely to be co-administered with rivaroxaban in AF are known CYP3A4/2J2 and/or P-gp inhibitors (Wessler *et al.*, 2013; US FDA, 2017). Furthermore, given that the prevalence of AF burgeons in the elderly population (Chugh *et al.*, 2014), assessing the implications of age-related physiological decline on the extent of these clinically relevant DDIs also becomes essential to guide pharmacotherapy. Nevertheless, practical constraints often restrict the number of dedicated trials that can be conducted to evaluate all clinically plausible

permutations. Consequently, physiologically-based pharmacokinetic (PBPK) modeling has emerged as a valuable tool in the quantitative rationalization of PK variabilities due to complex DDDIs.

By coupling the defining properties of rivaroxaban and the biological system with trial design, minimal PBPK models developed by Grillo *et al.* (Grillo *et al.*, 2012) and Ismail *et al.* (Ismail *et al.*, 2018) have prospectively established clinically significant DDDIs between rivaroxaban and erythromycin or verapamil in renally impaired patients. Findings were instrumental in substantiating cautionary language discouraging concomitant administration of rivaroxaban with moderate CYP3A4/P-gp inhibitors in patients with renal dysfunction (US FDA, 2011b). Nevertheless, subsequent model verification using clinical DDI data uncovered a key limitation of the current minimal PBPK models where major physiological compartments (except the liver) are combined with the plasma compartment. While these PBPK models incorporated interactions comprising both CYP3A4 and P-gp pathways, clinical urinary excretion data revealed negligible decreases in the renal clearance of rivaroxaban when it was co-administered with either erythromycin or verapamil in healthy patients (Moore *et al.*, 2014; Greenblatt *et al.*, 2018). This invalidated the initial assumption of a transporter-mediated component mediating the observed DDDI. Hence, to justify PBPK-guided extrapolation beyond the clinical trial population in the investigation of potential DDDIs involving rivaroxaban, mechanistic delineation of passive and active processes governing the renal clearance of rivaroxaban becomes essential.

Consequently, this study aims to develop and verify a full PBPK model for rivaroxaban, via incorporation of both *in vivo* clinical PK data as well as *in vitro* experimental measurements, which can be utilized to inform drug-specific parameters through *in vitro* to *in vivo* extrapolation (IVIVE). Upon successful recapitulation of observed rivaroxaban PK and urinary excretion profiles in both healthy and renal impaired patients, *in vitro* inhibitory parameters utilizing rivaroxaban as the probe substrate would be quantified and employed in retrospective DDI simulations linking rivaroxaban with prototypical CYP3A4/2J2 and P-gp inhibitors (ketoconazole and verapamil which yield different quantitative effects on the renal clearance of rivaroxaban). We envision that this systematic approach to PBPK model verification would eventually instill confidence in acting on model-generated insights to support the

rational dose selection of rivaroxaban in previously untested, albeit realistically complex clinical scenarios. The long-term aim is to minimize inadvertent increases in the systemic exposure of rivaroxaban while preserving its anticoagulant efficacy.

MATERIALS AND METHODS

The workflow schematic adopted for PBPK model development, verification and iterative refinement is illustrated in **Fig. 1**. Mechanistic modeling of permeability and transport kinetics was implemented with the Simcyp *In Vitro* Analysis (SIVA) toolkit (Version 3). All PK simulations presented herein were conducted using a population-based absorption, distribution, metabolism and excretion simulator (version 17, Simcyp®, Sheffield, UK).

1.1 Model Development

PBPK Model of Rivaroxaban. Key drug-dependent parameters necessary for simulation of the kinetics of rivaroxaban are delineated in **Table 1**. Oral absorption of rivaroxaban was predicted with the Advanced Dissolution, Absorption, Metabolism (ADAM) model implemented in Simcyp. The effective permeability of rivaroxaban in human ($P_{eff,man}$) was derived from *in vitro* apparent permeability (P_{app}) measured in Caco-2 cell monolayers (Gnoth *et al.*, 2011) using the P_{app}-P_{eff} correlation model within the simulator. Upon defining its intrinsic solubility (S_0) (Takács-Novák *et al.*, 2013), the dissolution rate of rivaroxaban was estimated with the diffusion layer model developed by Wang and Flanagan (Wang and Flanagan, 1999). The effects of bile on the *in vivo* solubility estimated in each segment of the gastrointestinal tract was quantified via the bile micelle:water partition coefficient ($K_{m:w}$), calculated from the predefined log P via a quantitative structure activity relationship model developed by Glomme *et al* (Glomme *et al.*, 2007). Simulated solubility outputs were compared with experimental biorelevant solubility measurements (Takács-Novák *et al.*, 2013) and $K_{m:w}$ was manually adjusted to achieve concordance. Subsequently, a whole body PBPK model was applied to describe the distribution of rivaroxaban, where tissue to plasma distribution equilibrium ratios (K_p) were calculated via mechanistic tissue composition equations developed by Rodgers and Rowland (Rodgers and Rowland, 2006). The volume of distribution at steady state (V_{ss}) was predicted to be 0.2 L/kg, which is lower than the observed *in vivo* V_{ss} of approximately 0.62 L/kg (Mueck *et al.*, 2014). Hence, a K_p scalar (applied equally to all tissues) of 2.2 was applied to optimize V_{ss}.

DMD Fast Forward. Published on September 10, 2019 as DOI: 10.1124/dmd.119.086918
This article has not been copyedited and formatted. The final version may differ from this version.

Hepatic Metabolism. Apparent oral and renal clearance (CL/F and CL_R) data were collated from primary literature sources following administration of rivaroxaban to healthy adult subjects (**Supplemental Table 1**). Overall weighted mean clearances were calculated using **eq. 1**.

$$W\bar{X} = \frac{\sum_{j=1}^{J} n_j . \bar{x}_j}{\sum_{j=1}^{J} n_j} \quad (\mathbf{1})$$

where $W\bar{X}$ is the weighted mean, n_j is the number of subjects in the jth study, and x_j is the mean of the jth study. Here a "study" is defined as the data associated with a group of subjects being administered a specific dose and dosing regimen of rivaroxaban, on a particular occasion, with "n" number of subjects. Based on a fractional metabolism in the liver of 0.37 for CYP3A4 and 0.29 for CYP2J2 as reported by Grillo *et al* (Grillo *et al.*, 2012), the unbound intrinsic clearances (CLu_{int}) of rivaroxaban mediated by CYP3A4 and CYP2J2 were derived from the weighted mean of CL/F after accounting for the contribution of CL_R, via retrograde application of the well-stirred model.

Mechanistic Kidney Model Development. The differential contribution of the primary processes governing the renal disposition of rivaroxaban (i.e. glomerular filtration, tubular secretion and tubular reabsorption) was quantified via by the mechanistic kidney model (MechKiM) within the simulator. *In vitro* transport assays investigating the P-gp-mediated efflux kinetics of rivaroxaban were first performed in Madin Darby canine kidney (MDCK) subclone I cells transfected with multidrug resistance protein (MDR1). To account for the bidirectional passive permeability of rivaroxaban across the apical (A) and basolateral (B) membranes in addition to apical P-gp-mediated efflux driven by unbound intracellular rivaroxaban concentrations, time- (60-420 min) and concentration- (3-100 µM donor rivaroxaban) dependent data, measured in the absorptive (A to B) direction, were fitted to a mechanistic model that dynamically simulates flux in rivaroxaban concentrations within the apical, basolateral and intracellular compartments of the transwell apparatus. Derived *in vitro* estimates of the maximum rate of active transport (J_{max}), Michaelis constant (K_m) and passive permeability (P_{pass}) were subsequently subjected to quantitative IVIVE scaling as highlighted in **eqs. 2** and **3** to simulate the

DMD Fast Forward. Published on September 10, 2019 as DOI: 10.1124/dmd.119.086918
This article has not been copyedited and formatted. The final version may differ from this version.

intrinsic clearance attributed to *in vivo* P-gp-mediated tubular secretion ($CLu_{int,T\ per\ kidney}$) and passive diffusion clearances ($CL_{PD,kidney}$) that contribute to tubular reabsorption respectively.

$$CLu_{int,T\ per\ kidney} = \frac{J_{max}}{K_{m,u}} / CL_{u,int} \times REF_{PTC} \times PTCPGK \times kidney\ weight \quad (2)$$

$$CL_{PD,kidney} = \frac{P_{pass} \times Nephron\ Surface\ Area\ based\ on\ 2\ kidneys}{PTCPGK \times kidney\ weight} \quad (3)$$

In **eq. 2**, J_{max} (pmol/min) generated was first normalized to protein concentration in each transwell insert, quantified using the BCA protein assay. J_{max} was subsequently converted from pmol/min/mg protein to pmol/min/10^6 cells based on 1 million MDCK cells containing 0.08 mg of total protein (Scotcher *et al.*, 2017). Differential P-gp mRNA expression data in the kidney, intestine and MDCK cells was used to inform the relative expression factor (REF_{PTC}) (Scotcher *et al.*, 2017). In **eq. 3**, total nephron surface area (291 cm^2), kidney weight (341.5 g) and the number of proximal tubular cells per gram kidney, PTCPGK (60 million in a healthy population) were used as IVIVE scaling factors to convert *in vitro* P_{app} to CL_{PD} (Emami Riedmaier *et al.*, 2016).

Further details on the chemicals, culture techniques, modeling and fitting procedures used are highlighted in **Supplemental Methods Section 1.1**.

PBPK Models of Inhibitors (Ketoconazole and Verapamil). Ketoconazole, verapamil and its primary metabolite, norverapamil, are prototypical CYP3A4/2J2 as well as P-gp inhibitors that have been implicated in clinical DDIs with rivaroxaban (Mueck *et al.*, 2013; Greenblatt *et al.*, 2018). In the construction of PBPK-DDI models, the verified compound file of ketoconazole provided in Simcyp® (version 17) was used. In the case of verapamil, although the compound file provided in Simcyp® (version 17) allowed adequate modeling of the PK profile of an immediate release formulation, co-administration of rivaroxaban and sustained release verapamil capsules in the trial by Greenblatt *et al* necessitated further refinement of verapamil's absorption kinetics. As described in **Supplemental Fig.**

1, a sequential one stage convolution procedure was implemented that models the relationship between the *in vitro* dissolution profile and the observed plasma concentration-time profile of verapamil. Final model parameters for ketoconazole and verapamil are summarized in **Supplemental Tables 2.1-2.3.**

2.1 Model Verification – PK Simulations

Verification of Basal PBPK Model of Rivaroxaban and Verapamil. PK profiles following single or multiple administration of clinically relevant doses to healthy subjects using the default healthy 'NEurCaucasian" population available within Simcyp were first simulated to verify the performance of the PBPK models of rivaroxaban and verapamil. During the model verification process, the population, number of participants, dose and regimen selected for the simulations were matched to the corresponding clinical study designs (**Supplemental Table 3**). A total of 10 trials were simulated to assess variability across groups. The predictive accuracies of the PBPK models were evaluated via visual predictive checks against average plasma concentration-time data digitized using a WebPlotDigitizer (version 4.0, https://automeris.io/WebPlotDigitizer). Additionally, a metric approach detailed by Abduljalil *et al.* that considers both the intrinsic variability of observed PK parameters (i.e. area under the curve, AUC; peak plasma concentration, C_{max}) as well as the clinical sample size was also applied to assess simulated values (Abduljalil *et al.*, 2014).

Simulation of Rivaroxaban's CL_R Using the Mechanistic Kidney Model in a Healthy Population and in Patients with Mild Renal Impairment. Simulations of rivaroxaban's plasma concentration-time and urinary excretion profiles in a healthy population using the final mechanistic model were first compared with the PBPK model of rivaroxaban where weighted mean CL_R collated from 7 independent studies was defined as a single input parameter (**Supplemental Table 1**). Upon verification of the predictive capabilities of the mechanistic kidney model in healthy subjects, system-dependent parameters within the model were further modified to reflect potential physiological changes synonymous with renal impairment. Based on the intact nephron hypothesis (INH) by Bricker, damaged nephrons stop working completely while undamaged nephrons function normally (Bricker, 1969). Consequently, proportional reductions in tubular secretion and glomerular filtration would likely be

observed in chronic kidney disease (CKD). In this study, a decline in PTCPGK was utilized to represent the loss of tubular cells and hence active secretion that is consistent with the INH concept. Consequently, the default value of 60 million PTCPGK corresponding to the representative GFR of a healthy population (136.4 mL/min) was scaled down proportionally to 28.6 million according to the median GFR that occurs in mild renal impairment (GFR= 65 mL/min in a range of 50 to 79 mL/min) (Scotcher *et al.*, 2017; Hsueh *et al.*, 2018) (**Supplemental Table 4**). This newly defined population was subsequently used to predict the observed attenuations in rivaroxaban's CL_R in mild renal impairment (**Supplemental Methods, Modelling Supplemental Data File 1**).

2.2 Model Verification – Retrospective DDI Simulations

Upon accurate recapitulation of rivaroxaban's PK, performance verification in both the uninhibited and inhibited states is essential to ascertain that rivaroxaban has been adequately characterized as a DDI victim (Shebley *et al.*, 2018). Hence, PBPK-DDI models were constructed via the incorporation of *in vitro* inhibitory parameters describing the inhibitory potential of verapamil, norverapamil and ketoconazole against the CYP3A4/2J2-mediated metabolism as well as P-gp-mediated secretion of rivaroxaban (**Supplemental Methods Section 2, Modelling Supplemental Data Files 2 and 3**). For DDI simulations, statistical analyses were performed using SPSS Version 22. AUC, C_{max} and CL of rivaroxaban were analyzed assuming log normally distributed data. Student's t test was used to analyze the difference in these parameters in the absence and presence of concomitant inhibitors. Point estimates and exploratory 90% confidence intervals (CIs) for the ratios were calculated by retransformation of the logarithmic results. Based on these analyses, a refined predictive measure proposed by Guest *et al.* incorporating PK variability coupled with variable prediction boundaries dependent on the extent of interaction was applied in defining the success of DDI simulations (Guest *et al.*, 2011).

3 Model Refinement

Incorporation of Organic Anion Transporter 3 (OAT3)-Mediated Basolateral Uptake of Rivaroxaban. Consideration of glomerular filtration, tubular reabsorption via passive permeability clearances and apical P-gp-mediated secretion resulted in an underestimation of rivaroxaban's CL_R,

alluding to potential undefined mechanisms governing rivaroxaban's renal disposition. Tsuruya *et al.* reported the specific uptake of rivaroxaban in mouse OAT3-expressing cells, with J_{max} and K_m in mOAT3-transfected cells determined to be 72.9 ± 46.8 pmol/min/mg protein and 1.01 ± 0.70 µM respectively (Tsuruya *et al.*, 2017). In the absence of transporter abundance or expression to facilitate allometric scaling, rivaroxaban uptake was independently investigated in this study using hOAT3-transfected HEK cell lines obtained from Dr. Kathleen Giacomini (University of California, San Francisco, CA). Details on the culture techniques, uptake assay protocol, two compartmental modeling and fitting procedures are highlighted in **Supplemental Methods Section 1.1**. Derived *in vitro* active uptake clearance (CL_{int}) was similarly subjected to IVIVE using **eq. 3**. correcting for measured protein (0.15 mg) per million HEK cells. An alternative top-down approach was further utilized to estimate the CLu_{int} governing OAT3-mediated uptake. Using sensitivity analysis optimization, the CLu_{int} was determined to be the value producing a simulated CL_R that converged with the weighted mean CL_R of 3.1L/h when serum creatinine was fixed at 80 µmol/L (corresponding to GFR = 120 mL/min in healthy volunteers) (Scotcher *et al.*, 2017).

RESULTS

1 Development and Verification of the PBPK Models of Rivaroxaban and Verapamil

Basal PBPK Model of Rivaroxaban Recapitulated Clinically Observed PK Profiles. The weighted mean CL/F and CL_R of rivaroxaban collated from 7 independent studies in healthy volunteers were 8.6 L/h and 3.1 L/h respectively (**Supplemental Table 1**). Using the retrograde model, CLu_{int} attributed to CYP2J2 and CYP3A4 were calculated to be 5.69 and 0.064 µL/min/pmol of isoform, with additional liver clearance defined to be 23.5 µL/min/mg of liver microsomal protein. The effect of food in enhancing rivaroxaban's bioavailability at the 20 mg dose strength was recapitulated by considering the differential influences of fasted versus fed conditions on the extent of bile micelle-mediated solubilization (**Fig. 2A**, **Table 2**). As highlighted in **Table 2**, simulated geometric mean AUC was 1512 µg.h/L in the fasted state compared to 2127 µg.h/L in the fed state. This predicted 1.41-fold increase in the presence of food was aligned with the 1.39-fold change observed in a Phase I confirmatory food effect trial (Stampfuss *et al.*, 2013). Model predictive performance was further assessed using external verification datasets from independent clinical trials not utilized in model development. Plasma concentration-time profiles of 10 mg (**Fig. 2B**) and 20 mg (**Fig. 2C**) doses of rivaroxaban (**Modelling Supplemental Data File 4**) compared well with the reference published studies by Mueck *et al.* and Greenblatt *et al* (Mueck *et al.*, 2013; Greenblatt *et al.*, 2018) respectively, with observed PK parameters (AUC, C_{max} and CL) falling within the pre-specified PK prediction criteria (**Table 2**).

Three-Compartmental Analysis Enabled Accurate Determination of Kinetic Constants Governing the *In Vitro* P-gp-Mediated Efflux of Rivaroxaban. Approximately one third (36%) of the absorbed dose of rivaroxaban is excreted unchanged in the kidney, with active tubular secretion accounting for 30% (Mueck *et al.*, 2013). As a result, accurate estimation of kinetic parameters governing the P-gp-mediated efflux of rivaroxaban based on *in vitro* data is critical for successful IVIVE of its renal disposition. Preliminary analyses of bidirectional MDCK-MDR1 transport assays via the conventional Michaelis-Menten approach established time-linear conditions for both absorptive (**Supplemental Fig. 2A**) and basolateral rivaroxaban transport (**Supplemental Fig. 2B**) as well as the

superior sensitivity of absorptive flux (**Supplemental Fig. 2C**) compared to basolateral flux (**Supplemental Fig. 2D**) in response to apical P-gp efflux activity. Yet, as seen in **Supplemental Fig. 2C**, solubility limitations prevented saturation of rivaroxaban transport in the absorptive direction. Hence, to account for the interaction of P-gp with unbound intracellular concentrations of rivaroxaban, mechanistic three-compartmental modeling was subsequently applied to analyze both time- and concentration-dependent data describing rivaroxaban's absorptive transport. Unbound rivaroxaban concentrations in the extracellular (fu_{media}) and intracellular (fu_{cell}) compartments, determined via ultrafiltration experiments to be 1 and 0.023 respectively, were incorporated as fixed drug-dependent parameters (**Supplemental Table 5**). $J_{max,app}$ and $K_{m,app}$ (97.98 pmol/min and 836.8 µM respectively) determined using the conventional Michaelis Menten approach were also utilized as *a priori* information for naïve pooled fitting via both hybrid and local (Nelder Mead) optimization procedures. As highlighted in **Table 3**, the convergence of J_{max} and K_m estimates from two different optimization methods attested to the robustness of the three-compartmental approach and established that fitting outcomes were minimally influenced by initial J_{max} and K_m values. Visual predictive checks also demonstrated consistency between experimental measurements and simulated rivaroxaban concentration-time profiles in the basolateral compartment (**Fig. 3A** and **B**). Given that Nelder Mead optimization resulted in lower Akaike information criterion (AIC) and difference in small sample size corrected version of AIC (ΔAIC_c) values, J_{max} = 37.83 pmol/min, K_m = 9.42 µM and P_{pass} = 12.88 × 10^6 cm/s were subjected to quantitative IVIVE via **eqs. 2** and **3** to generate $CLu_{int,T\ per\ kidney}$ (J_{max} = 80.921 pmol/min/10^6 cells and $K_{m,u}$ = 9.42 µM) and $CL_{PD,kidney}$ (1.09 × 10^{-5} µL/min/10^6 cells)for parameterization of the mechanistic kidney model (**Table 1**).

IVIVE of Rivaroxaban's Renal Clearance Revealed the Pivotal Role of Basolateral Uptake. Using the mechanistic kidney model, the relative contribution of various processes (i.e. glomerular filtration, tubular reabsorption and active secretion) involved in rivaroxaban's renal excretion clearance was assessed in a stepwise manner. Expectedly, consideration of either glomerular filtration in isolation or both glomerular filtration and passive tubular reabsorption resulted in a substantial underprediction of rivaroxaban's CL_R (predicted CL_R of 0.41 and 0.36 L/h respectively) (**Fig. 4A**) and a corresponding

overestimation of its systemic exposure (**Fig. 4B**), underscoring the significance of active renal secretion in mediating rivaroxaban's renal disposition. However, sole incorporation of P-gp-mediated apical efflux demonstrated marginal effects on both CL_R and systemic exposure (**Fig. 4A** and **B**). As highlighted in **Table 4**, without OAT3-mediated basolateral uptake, CL_R was underpredicted by 85% and the predicted AUC was 1.51-fold higher than that reported by Greenblatt *et al.*, falling outside the prespecified success criteria (Greenblatt *et al.*, 2018). Hence, this provided the impetus for mechanistic investigation of OAT3-mediated rivaroxaban uptake.

Kinetic Constants Governing *In Vitro* OAT3-Mediated Uptake of Rivaroxaban were Comparable to Top-Down Estimates of OAT3-Mediated Intrinsic Clearance. Upon establishing the functionality of the OAT3/OAT1-transfected systems (**Supplemental Fig. 3A** and **3B**), preliminary investigation of potential rivaroxaban uptake was performed. The uptake of rivaroxaban by hOAT3-expressing cells was higher than that by the empty-vector transfected cells at 5 min and was further inhibited by a prototypical OAT inhibitor, probenecid (50 μM) (**Supplemental Fig. 3C**). In contrast, the uptake of rivaroxaban by hOAT1-expressing cells was comparable to that of the empty vector transfected cells at 5 min (**Supplemental Fig. 3D**). Taken together, rivaroxaban is a substrate of hOAT3 but not hOAT1. Time-dependent rivaroxaban uptake was subsequently evaluated, and linearity was preserved up to 2 min (**Supplemental Fig. 3E).** Consequently, concentration-dependent transport of rivaroxaban (0.5-100 μM) was investigated under time-linear conditions in both wild type and OAT3-transfected cells (**Supplemental Fig. 3G**). Total rivaroxaban uptake (solid black line, **Supplemental Fig. 3H**) was fitted via the conventional two-step approach (**eq. S14**). Accounting for passive diffusion (**Supplemental Fig. 3F**), calculated to be 22.65 μL/min/10^6 cells, saturable active uptake (grey solid line) was observed with transporter-mediated intrinsic clearance ($CL_{int,T}$) estimated to be 33.91 μL/min/10^6 cells (**Supplemental Fig. 3H**). Given that data from 2 min incubations have been shown to produce large standard errors in the estimation of CL_{PD} (Menochet *et al.*, 2012), $CL_{PD,kidney}$ (1.09×10^{-5} μL/min/10^6 cells obtained previously via IVIVE scaling) and $CL_{int,T}$ derived from the two step approach were eventually utilized as initial estimates for naïve pooled fitting of measured time-and concentration-dependent data via two-compartmental modeling. Visual predictive checks demonstrated consistency between experimental

DMD Fast Forward. Published on September 10, 2019 as DOI: 10.1124/dmd.119.086918
This article has not been copyedited and formatted. The final version may differ from this version.

measurements and simulated intracellular rivaroxaban concentration-time profiles (**Fig. 3C** and **D**). OAT3 $CLu_{int,T}$ was determined to be 41.33 µL/min/10^6 cells (**Table 3**) and compared well with estimates obtained via a sensitivity analysis-based approach that simulated variations in rivaroxaban's CL_R as a function of OAT3 $CLu_{int,T}$ and serum creatinine input parameter values. The optimal $CLu_{int,T}$ for uptake governed by OAT3 (43 µL/min/10^6 cells) was taken at the intersection of the simulated rivaroxaban CL_R with the observed weighted CL_R of 3.1 L/h (green plane) at a serum creatinine of 80 µmol/L (which corresponds to simulated GFR∼120 ml/min in healthy volunteers) (**Supplemental Fig. 4**).

Concurrent Basolateral Uptake and Apical Efflux were Necessary to Recapitulate Rivaroxaban's Renal Clearance. The optimized $CLu_{int,T}$ of OAT3 mediated uptake was incorporated into the mechanistic kidney model. In a hypothetical scenario where basolateral OAT3 uptake was present but apical P-gp efflux was disregarded, although simulations managed to recapitulate the observed plasma concentration-time profile of rivaroxaban (**Fig. 4B**), the amount excreted unchanged in urine remained underestimated (**Fig. 4A** and **Table 4**). Hence, our simulations demonstrate that accounting for basolateral uptake in conjunction with apical efflux was crucial in ensuring that simulated plasma concentration-time (**Fig. 4B**) and urinary excretion rate profiles (**Fig. 4A**) matched the observed clinical data, with PK parameters (AUC, C_{max} and CL_R) satisfying the prespecified success criteria (**Table 4, Modelling Supplemental Data File 5**).

Simulations using the Mild Renal Impairment Population Adequately Predicted Increases in the Systemic Exposure of Rivaroxaban. Upon successful verification of the mechanistic kidney model in healthy subjects, which affirmed the accuracy of drug-dependent parameters defined for rivaroxaban, the ability of the PBPK model to predict the altered PK of rivaroxaban in mild renal impairment was subsequently investigated. With the application of INH, assuming proportional reductions in GFR and tubular secretion, simulated geometric mean rivaroxaban AUC and CL_R fold changes were 1.20-fold and 0.54-fold respectively (**Table 4**). These point estimates fell within the range of clinical success determined based on the clinically observed AUC and CL_R fold changes of 1.11 and 0.93 (**Table 4, Modelling Supplemental File 1**). Modeled plasma-concentration time profiles also reasonably

characterized the increase in rivaroxaban's systemic exposure with concomitant mild renal impairment (**Fig. 4C**).

PBPK Models of Immediate Release Verapamil and Norverapamil Recapitulated Clinically Observed PK Profiles. In the first step of the two stage IVIVC framework (**Supplemental Fig. 1**), using the verified verapamil and norverapamil compound files provided within the Simcyp simulator, simulated PK profiles following a single 80 mg immediate release dose of verapamil were aligned with the reference published study by Haeri *et al.* (**Fig. 5A**) (Haeri *et al.*, 2014). Additionally, the model effectively predicted the observed AUC data within the calculated prediction criteria (**Supplemental Table 6**). This affirms that *in vivo* disposition parameters were accurately defined before proceeding with IVIVC.

PBPK Models of Verapamil and Norverapamil Described Absorption Kinetics following Administration of a Sustained Release Formulation. IVIVC convolution was subsequently applied to predict the PK following administration of a single 120 mg dose of controlled release verapamil based on an initial *in vitro* dissolution input (**Fig. 5B**) (Wise, 2000). Simulated and observed plasma concentrations reported by Frishman *et al.* were compared and discrepancies prompted iterative refinement of dissolution parameters to produce an *in vivo* dissolution profile (**Fig. 5B**) that adequately described absorption kinetics following single dose administration of a sustained release verapamil capsule (**Fig. 5C**) (Frishman and Lazar, 1992). Accumulation of verapamil following multiple dosing (i.e. 120mg on day 1, 240mg on day 2 and 360mg from day 3 to day 10) was also in line with clinical data (**Fig. 5D**) (Greenblatt *et al.*, 2018).

2 Retrospective Simulations of Enzyme- and Transporter-Mediated DDIs between Rivaroxaban and Verapamil/Ketoconazole

Although preliminary PK simulations verified the predictive potential of the basal compound model of rivaroxaban, given that the PBPK model of rivaroxaban is intended to be applied for the characterization of complex DDIs involving potential enzyme-transporter interplay, it becomes essential to further

evaluate its predictive performance against observed DDIs with CYP3A4/2J2 and/or P-gp inhibitors (Shebley *et al.*, 2018).

DDDIs between Rivaroxaban and Verapamil were Successfully Modeled. The capability of verapamil and its major metabolite norverapamil to elicit both mechanism-based inactivation (MBI) as well as reversible inhibition of CYP3A4 has been established previously (Orr *et al.*, 2012). Nevertheless, in our study, *in vitro* inhibitory parameters (i.e. k_{inact}: the theoretical maximum inactivation rate constant at infinite inactivator concentration; K_I: the inactivator concentration yielding an inactivation rate at half of k_{inact} and K_i: the equilibrium dissociation constant for the enzyme inhibitor complex) were quantified using rivaroxaban as probe substrate.

Collectively, *in vitro* inhibition studies affirmed the MBI (**Supplemental Fig. 5A-D**) and reversible inhibition (**Supplemental Fig. 6A-D**) of CYP3A4-mediated metabolism of rivaroxaban by verapamil and norverapamil. A summary of the *in vitro* inhibition parameters derived is presented in **Table 5**. Conversely, our preliminary studies suggest the absence of MBI of CYP2J2 by verapamil and norverapamil (**Supplemental Fig. 5E** and **5F**). Similarly, reversible inhibition by verapamil and norverapamil against CYP2J2 yielded large K_i values of 12.2 and 161.8 µM respectively (**Supplemental Fig. 6E-H**). R_1 ratios (**Table 5**) were both less than the threshold of 1.02 recommended by FDA, hence eliminating the need for further assessment of DDI potential.

Notably, despite a previous *in vitro* study demonstrating an inhibitory effect of verapamil against the P-gp-mediated efflux of rivaroxaban (**Table 5**) (Gnoth *et al.*, 2011), *in vivo* data revealed that the amount of rivaroxaban excreted unchanged in urine was elevated in the presence of verapamil (Greenblatt *et al.*, 2018). This *in vitro in vivo* disconnect alluded to the negligible role of transporters in perpetrating the eventual DDI between rivaroxaban and verapamil. Subsequent assimilation of derived CYP3A4 inhibitory parameters into the PBPK-DDI model accurately recapitulated the observed DDI magnitude (**Fig. 6A**) and the increase in CL_R (**Fig. 6B**). Simulated geometric mean (90% CI) AUC and CL ratios of 1.46 (1.33, 1.61) and 0.68 (0.62, 0.75) were within the range of acceptable performance calculated based on the clinically observed AUC and CL-fold changes of rivaroxaban in the presence

of verapamil (**Table 6, Modelling Supplemental Data File 2**). In patients with underlying mild renal impairment, verapamil co-administration resulted in simulated geometric mean AUC and CL-fold changes of 1.70 and 0.59 respectively, meeting success criteria defined in **Table 6**, hence attesting to the ability of the PBPK-DDI model to accurately recapitulate an enzymatic DDDI scenario (**Fig. 6C**).

Extent of DDIs between Rivaroxaban and Ketoconazole was Underestimated Despite Consideration of CYP3A4, CYP2J2 and P-gp Inhibition. *In vitro* investigations verified the inhibition of CYP3A4, CYP2J2-mediated metabolism as well as P-gp-mediated efflux of rivaroxaban with co-administration of ketoconazole (**Supplemental Fig. 7A-F**). Simulated fold reduction in CL_H met the success criteria delineated in **Table 6**, reliably supporting conclusions that the extent of enzyme-mediated DDI was accurately reproduced. Nevertheless, as illustrated in **Fig. 6D**, the modeled plasma concentration-time profile in the presence of ketoconazole evidently demonstrated an underestimation of DDI magnitude (blue solid line). Moreover, PK parameters (AUC, C_{max} and CL_R) fell outside the prespecified acceptance criteria (**Table 6**), suggesting that the nature and potency of transporter-mediated interactions between rivaroxaban and ketoconazole have not been adequately elucidated. Results of a subsequent sensitivity analysis (**Supplemental Fig. 8A**) corroborated this postulation and demonstrated that sole inhibition of P-gp-mediated efflux is unlikely to substantially affect rivaroxaban's systemic exposure. In contrast, AUC-fold change was highly sensitive to inhibition of OAT3-mediated basolateral uptake. *In vitro* inhibition experiments further established inhibition of OAT3-mediated uptake by ketoconazole (IC_{50} = 15.77 μM) (**Supplemental Fig. 7G**). Nevertheless, direct incorporation of the measured *in vitro* K_i was unable to recapitulate the clinically observed DDI magnitude (data not shown) and further optimization of the K_i value of ketoconazole to 0.01 μM was eventually required (blue dashed line in **Fig. 6D, Table 6, Modelling Supplemental Data File 3**).

DISCUSSION

In the US, 30–50% of adverse drug reactions are due to dosing errors (Neely, 2017), largely implicating vulnerable populations that incidentally constitute the exclusion criteria of pivotal clinical trials (Darwich *et al.*, 2017). PBPK modeling has proven to be a panacea for the perennial challenge of suboptimal therapeutic outcomes in such complex and untested, albeit clinically relevant scenarios. Its unique ability to quantitatively integrate the multitude of drug- and system-dependent parameters, that can influence an individual's dose response, has guided refined dosing in multiple clinical applications, particularly involving DDIs and special populations (Sager *et al.*, 2015; Jamei, 2016).

Using PBPK modeling, Grillo *et al.* predicted clinically significant increases in rivaroxaban exposure due to renal impairment and moderate CYP3A4/P-gp inhibition by erythromycin (Grillo *et al.*, 2012). The findings informed current product labeling where concomitant use of rivaroxaban with a combined weak to moderate inhibitor of CYP3A4 and an inhibitor of P-gp and/or BCRP should be avoided under any degree of renal impairment. Given that such cautionary language hampers the utility of relevant drug combinations in AF management, Ismail *et al.* proposed dosing modifications in renal impairment and concomitant verapamil administration via correlating PBPK-predicted increases in rivaroxaban exposure with bleeding risk outcomes (Ismail *et al.*, 2018). Lastly, Xu *et al.* interrogated the exacerbation of rivaroxaban DDIs by hepatic dysfunction (Xu *et al.*, 2018).

Prior to application, a PBPK model must be qualified as fit for purpose (Shebley *et al.*, 2018) (**Fig. 1**). The four principal aspects essential for robust model qualification are namely, (1) evaluating model relevance to research context; (2) assessing sources of uncertainty and implications; (3) capturing known variabilities in clinical outcomes; and (4) ensuring that model results are qualitatively and quantitatively consistent with test data (Friedrich, 2016). Fulfilling the third and fourth criteria, the abovementioned and our developed models demonstrated qualitative and quantitative reproduction of rivaroxaban's essential clinical PK characteristics, such as rapid and near complete oral absorption, dose proportional increases in rivaroxaban exposure under fed conditions (**Fig. 2B** and **2C**), lack of

accumulation upon multiple dosing (Kubitza, Becka, Voith, *et al.*, 2005; Kubitza, Becka, Wensing, *et al.*, 2005; Zhao *et al.*, 2009), and true representation of interindividual variability (Jamei *et al.*, 2009); (US FDA, 2011a). Nevertheless, the intended application of the PBPK model of rivaroxaban to the interrogation of DDIs importantly entails that the first and second criteria are also adequately satisfied. Ensuring that the model scope is sufficiently mechanistic in delineating **1)** the renal disposition of rivaroxaban and **2)** inhibition of the metabolic/transport pathways of rivaroxaban elimination, is required to facilitate rigorous identification and assessment of biological uncertainties that may result in incongruities between predictions and actual outcomes.

Our PBPK model is novel and mechanistically detailed in parameterizing the renal disposition of rivaroxaban. Previously, its CL_R was defined as a function of glomerular filtration and net secretion (calculated as the difference between absolute secretion and absolute reabsorption) (Grillo *et al.*, 2012; Ismail *et al.*, 2018; Xu *et al.*, 2018). Conflating these distinct processes precludes mechanistic characterization of their differential contributions to CL_R of rivaroxaban. Additionally, by ascribing renal elimination of rivaroxaban to the apparent plasma compartment (i.e. minimal PBPK model), both Grillo *et al.* and Ismail *et al.* were unable to predict urinary excretion data for direct assessment of model-predicted CL_R. The significance of such mechanistic detail is further underscored with *in vitro* evidence demonstrating how consideration of P-gp-mediated efflux and passive permeability produced adequate fits for high permeability compounds (e.g. amprenavir and quinidine) but not for low permeability substrates (e.g. loperamide and digoxin) (Acharya *et al.*, 2008). For loperamide and digoxin, observed efflux kinetics were substantially greater than could be fitted by passive permeability alone and improvement in fitting outcomes was contingent on the addition of a basolateral uptake transporter (Acharya *et al.*, 2008). Consistently, evaluating the extent of passive permeability becomes diagnostic for the kinetic necessity of basolateral uptake (Lumen *et al.*, 2013; Huang and Isoherranen, 2018). In this study, incorporating passive permeability (P_{pass} = 12.88 × 10^{-6} cm/s, **Table 3**) estimates from three-compartment modeling yielded a CL_{PD} of 1.09 × 10^{-5} μL/min/10^6 cells when scaled using tubular surface area. When considered in tandem with P-gp efflux kinetics (**Table 3**), the clinically observed CL_R of rivaroxaban remained underestimated by our simulation (**Fig. 4A**). Nevertheless,

without independent verification of specific model assumptions governing passive diffusion clearance in the kidneys, it is inevitable that certainty in the quantitative contribution of active transport to renal clearance remains low and interdependent on the error in predicted diffusion clearance (Huang and Isoherranen, 2018). Hence, using a 35-compartment mechanistic kidney model developed by Huang and Isoherranen, where *in vitro* to *in vivo* predictions of renal clearance using plasma unbound fraction and permeability data have been systematically verified for a set of 46 compounds (Huang and Isoherranen, 2018), we demonstrate that renal clearance predicted via MechKiM in the Simcyp simulator was within twofold of that simulated using the 35-compartment model when a P_{pass} of 12.88 $\times 10^{-6}$ cm/s was incorporated (**Supplemental Table 8**), verifying the passive diffusion component of the mechanistic kidney model constructed for rivaroxaban in this study.

With a verified passive diffusion process, the inability to recapitulate the CL_R of rivaroxaban can be thus be confidently attributed to the presence of knowledge gaps in transporter-mediated clearance that imposes constraints on the exclusive utilization of bottom-up approaches. In such scenarios, the utility of a middle-out approach has received increasing recognition (Rostami-Hodjegan, 2018). Using reverse translational modeling, clinical data of rivaroxaban obtained with co-administration of ketoconazole revealed surprising fold reductions in Vd/F (0.53) in addition to CL/F (0.39), such that half-life was minimally affected (US FDA, 2011a). Coupled with experimental demonstration of rivaroxaban uptake in human OAT3 expressing cells, the convergence of evidences reinforces the plausibility of our postulated renal basolateral uptake process. Sensitivity analyses in this study further underscored the relative insensitivity of observed CL_R to P-gp REF (**Supplemental Fig. 8B**) and confirmed that sole inhibition of P-gp-mediated efflux is unlikely to produce significant increases in rivaroxaban's systemic exposure (**Fig. 6D**, **Supplemental Fig. 8A**). Hence, it becomes apparent that reliable quantitative extrapolation of *in vitro* derived OAT3-mediated J_{max} and K_m is essential to accurately define the renal excretion of rivaroxaban. With the emergence of quantitative transporter abundance data in kidney samples (reported OAT3 abundance of 3.5 ± 1.6 pmol/mg of total membrane protein) (Prasad *et al.*, 2016), IVIVE scaling factors can be accurately determined, removing the need for top down

optimization (**Supplemental Fig. 4**) where estimates of OAT3 CLu_{int} may be biased based on the mean CL_R and serum creatinine parameters defined.

Acknowledging the pivotal role of basolateral uptake in mediating the renal disposition of rivaroxaban enables informed analysis of the likelihood of observing transporter-mediated DDIs with rivaroxaban. A case in point would be verapamil, a known P-gp inhibitor that demonstrated *in vitro* inhibition of rivaroxaban's efflux in L-MDR1 cells (Gnoth *et al.*, 2011; US FDA, 2017). However, concomitant verapamil administration did not result in significant decrease in rivaroxaban's renal clearance, as highlighted in a DDI study by Greenblatt *et al* (Greenblatt *et al.*, 2018). This observation is substantiated by verapamil having a high mOAT3 K_i value of 31 µM (Ahn *et al.*, 2009). Consistently, our *in vitro* experiments also demonstrated negligible inhibition of OAT3-mediated uptake of rivaroxaban by verapamil up to 100 µM (**Supplemental Fig. 7H**). Furthermore, examining the drugs that have been shown to produce significant transporter-mediated DDIs with rivaroxaban (i.e. ketoconazole and ritonavir) (Mueck *et al.*, 2013) revealed *in vitro* evidence of OAT3 inhibition. Both ketoconazole and ritonavir inhibit estrone sulfate transport in transfected HEK-OAT3 cell lines (IC_{50} = 0.86 and 8.1 µM for ketoconazole and ritonavir respectively) (Vermeer *et al.*, 2016; Shebley *et al.*, 2017). When rivaroxaban was used as the probe substrate in this study, uptake inhibition by ketoconazole was also observed (**Supplemental Fig. 7G**). Nevertheless, further optimization of the K_i value of ketoconazole was required to recapitulate the clinically observed DDI magnitude (**Fig. 6D, Table 6**). Our observed underprediction in transporter K_i remains aligned with previous attempts to recapitulate transporter-mediated DDIs for solute carriers (Hsu et al., 2014; Burt et al., 2016). Such incongruity may reflect the incorrect assumption of a competitive mode of inhibition. Additionally, although the assumed concentration for inhibition (that added to the incubation media) should be largely consistent with that at the transporter binding site, the lipophilic nature of ketoconazole could have resulted in non-specific binding processes both *in vitro* and *in vivo*, further confounding interpretation of the inhibition data. Given that drugs that are likely to be co-administered with rivaroxaban have been reported to be P-gp inhibitors with unknown effects on OAT3-mediated uptake (e.g. amiodarone), elucidating the dynamic

interplay between apical P-gp efflux and basolateral OAT3 uptake using alternative approaches such as double-transfected cell lines with rivaroxaban as probe substrate becomes imperative.

Our second novelty lies in our adoption of rivaroxaban as the probe substrate when quantifying inhibition of metabolic and/or transport processes by verapamil and ketoconazole. In the previous PBPK-DDI model developed by Grillo *et al.*, a K_i value of 11 μM derived from an *in vitro* study using digoxin as substrate was utilized to describe the inhibitory potential of erythromycin on the P-gp-mediated efflux of rivaroxaban (Grillo *et al.*, 2012). However, Gnoth *et al.* reported that the directed efflux of rivaroxaban across P-gp-overexpressing L-MDR1 cells was unaffected by erythromycin (Gnoth *et al.*, 2011). A clinical DDI study by Moore *et al.* further demonstrated negligible inhibition of the active renal secretion of rivaroxaban by erythromycin (Moore *et al.*, 2014), underscoring how the nature and potency of DDIs are often unique to each substrate-inhibitor pair. This probe substrate specificity was similarly reflected in our *in vitro* experiments. For instance, verapamil has been reported to exhibit reversible inhibition against CYP2J2 when index substrates were used (Lee et al., 2012; Ren et al., 2013), but yielded minimal inhibition against CYP2J2-mediated metabolism of rivaroxaban (**Supplemental Fig. 6 E-H** and **Table 5**). Additionally, the *in vitro* MBI potencies of verapamil and norverapamil against CYP3A4 using index substrates were less potent (k_{inact}/K_I ratios of 0.9 and 1.74 $h^{-1}\mu M^{-1}$ respectively) than our experimentally derived parameters when rivaroxaban was used as the probe substrate (k_{inact}/K_I ratio of 2.37 and 8.59 $h^{-1}\mu M^{-1}$ respectively) (**Supplemental Table 7**). Finally, the *in vitro* reversible inhibition potency of ketoconazole against CYP3A4 using index substrate was more potent (K_i of 0.015 μM) than our experimentally measured potency using rivaroxaban as substrate (K_i of 0.094 μM) (**Supplemental Table 7**). Hence, it is evident that accurate recapitulation of enzyme-mediated and transporter-mediated DDIs involving rivaroxaban is contingent on generating reliable *in vitro* inhibitory estimates for parameterization of the PBPK-DDI model.

The future intended application of the current PBPK model of rivaroxaban is in extrapolation to untested scenarios implicating both enzyme- and transporter-mediated DDDIs. Assuming the INH and investigating the effect of mild renal impairment alone, our simulated AUC and CL_R fold changes of

rivaroxaban fell within predefined success criteria (**Table 4, Fig, 4C**). Additionally, as presented in **Supplemental Fig. 8C**, alterations in either PTCPGK or transporter abundance (**Supplemental Table 9**), two independent pathophysiological mechanisms that have been proposed to account for the reduction in tubular secretion (Naud *et al.*, 2011; Hsu *et al.*, 2014), yielded comparable effects on the renal clearance of rivaroxaban. Hence, it is conceptually reasonable to predict transporter-mediated DDDIs in mild-moderate CKD by empirically applying a scaling factor to account for the linear reduction in tubular secretion in accordance with GFR (either via PTCPGK or adjustment of transporter abundance) while accounting for inhibition against OAT3/P-gp-mediated transport. However, it is important to note that reductions of GFR and tubular secretion become disproportional in severe CKD, with the activity of OATs directly inhibited by uremic solutes at clinically relevant concentrations (Hsueh *et al.*, 2016, 2018), Although rivaroxaban is currently contraindicated in severe CKD (CrCL < 30 mL/min), the possibility of expanding rivaroxaban use to such patients has been raised (Dias *et al.*, 2016). Therefore, improved understanding of underlying mechanisms behind changes in tubular secretion in severe CKD is crucial.

In conclusion, the iteratively verified PBPK model of rivaroxaban is applicable to the investigation of enzyme and transporter-mediated DDDIs involving clinically relevant inhibitors and mild-moderate CKD, except in severe CKD where additional understanding of the effects of pathophysiology on transporter-mediated processes is required.

AUTHORSHIP CONTRIBUTIONS

Participated in research design:	Cheong, Teo, Chua and Chan
Conducted experiments:	Cheong, Teo and Chua
Performed data analysis:	Cheong, Teo, Chua and Chan
Wrote or contributed to the writing of the manuscript:	Cheong, Teo, Chua and Chan

REFERENCES

Abduljalil K, Cain T, Humphries H, and Rostami-Hodjegan A (2014) Deciding on success criteria for predictability of pharmacokinetic parameters from in vitro studies: An analysis based on in vivo observations. *Drug Metab Dispos* **42**:1478–1484.

Acharya P, O'Connor MP, Polli JW, Ayrton A, Ellens H, and Bentz J (2008) Kinetic Identification of Membrane Transporters That Assist P-glycoprotein-Mediated Transport of Digoxin and Loperamide through a Confluent Monolayer of MDCKII-hMDR1 Cells. *Drug Metab Dispos* **36**:452–460.

Ahn S-Y, Eraly SA, Tsigelny I, and Nigam SK (2009) Interaction of organic cations with organic anion transporters. *J Biol Chem* **284**:31422–30, American Society for Biochemistry and Molecular Biology.

Bricker NS (1969) On the meaning of the intact nephron hypothesis. *Am J Med* **46**:1–11.

Chugh SS, Havmoeller R, Narayanan K, Singh D, Rienstra M, Benjamin EJ, Gillum RF, Kim YH, McAnulty JH, Zheng ZJ, Forouzanfar MH, Naghavi M, Mensah GA, Ezzati M, and Murray CJL (2014) Worldwide epidemiology of atrial fibrillation: A global burden of disease 2010 study. *Circulation* **129**:837–847.

Darwich AS, Ogungbenro K, Vinks AA, Powell JR, Reny JL, Marsousi N, Daali Y, Fairman D, Cook J, Lesko LJ, McCune JS, Knibbe CAJ, de Wildt SN, Leeder JS, Neely M, Zuppa AF, Vicini P, Aarons L, Johnson TN, Boiani J, and Rostami-Hodjegan A (2017) Why has model-informed precision dosing not yet become common clinical reality? lessons from the past and a roadmap for the future. *Clin Pharmacol Ther* **101**:646–656.

Dias C, Moore KT, Murphy J, Ariyawansa J, Smith W, Mills RM, and Weir MR (2016) Pharmacokinetics, Pharmacodynamics, and Safety of Single-Dose Rivaroxaban in Chronic Hemodialysis. *Am J Nephrol* **43**:229–236.

Emami Riedmaier A, Burt H, Abduljalil K, and Neuhoff S (2016) More Power to OATP1B1: An Evaluation of Sample Size in Pharmacogenetic Studies Using a Rosuvastatin PBPK Model for Intestinal, Hepatic, and Renal Transporter-Mediated Clearances. *J Clin Pharmacol* S132–S142.

Friedrich CM (2016) A model qualification method for mechanistic physiological QSP models to support model-informed drug development. *CPT Pharmacometrics Syst Pharmacol* **5**:43–53.

Frishman WH, and Lazar EJ (1992) Sustained-release verapamil formulations for treating hypertension. *J Clin Pharmacol* **32**:455–62.

Glomme A, März J, and Dressman JB (2007) Predicting the Intestinal Solubility of Poorly Soluble Drugs. *Pharmacokinet Profiling Drug Res* 259–280.

Gnoth MJ, Buetehorn U, Muenster U, Schwarz T, and Sandmann S (2011) In vitro and in vivo P-glycoprotein transport characteristics of rivaroxaban. *J Pharmacol Exp Ther* **338**:372–380.

Greenblatt DJ, Patel M, Harmatz JS, Nicholson WT, Rubino CM, and Chow CR (2018) Impaired Rivaroxaban Clearance in Mild Renal Insufficiency With Verapamil Coadministration: Potential Implications for Bleeding Risk and Dose Selection. *J Clin Pharmacol* **58**:533–540.

Grillo JA, Zhao P, Bullock J, Booth BP, Lu M, Robie-Suh K, Berglund EG, Pang KS, Rahman A, Zhang L, Lesko LJ, and Huang S-M (2012) Utility of a physiologically-based pharmacokinetic (PBPK) modeling approach to quantitatively predict a complex drug-drug-disease interaction scenario for rivaroxaban during the drug review process: implications for clinical practice. *Biopharm Drug Dispos* **33**:99–110.

Guest EJ, Aarons L, Houston JB, Rostami-Hodjegan A, and Galetin A (2011) Critique of the two-fold measure of prediction success for ratios: application for the assessment of drug-drug interactions. *Drug Metab Dispos* **39**:170–3.

Haeri A, Javadian B, Saadati R, and Dadashzadeh S (2014) Metabolite parameters as an appropriate alternative approach for assessment of bioequivalence of two verapamil formulations. *Iran J Pharm Res IJPR* **13**:383–9, Shahid Beheshti University of Medical Sciences.

Hsu V, Vieira MDLT, Zhao P, Zhang L, Zheng JH, Nordmark A, Berglund EG, Giacomini KM, and Huang SM (2014) Towards quantitation of the effects of renal impairment and probenecid inhibition on kidney uptake and efflux transporters, using physiologically based pharmacokinetic modelling and simulations. *Clin Pharmacokinet* **53**:283–293.

Hsueh C-H, Yoshida K, Zhao P, Meyer TW, Zhang L, Huang S-M, and Giacomini KM (2016) Identification and Quantitative Assessment of Uremic Solutes as Inhibitors of Renal Organic Anion Transporters, OAT1 and OAT3. *Mol Pharm* **13**:3130–3140, American Chemical Society.

Hsueh CH, Hsu V, Zhao P, Zhang L, Giacomini KM, and Huang SM (2018) PBPK Modeling of the Effect of Reduced Kidney Function on the Pharmacokinetics of Drugs Excreted Renally by Organic Anion Transporters. *Clin Pharmacol Ther* **103**:485–492.

Huang W, and Isoherranen N (2018) Development of a Dynamic Physiologically Based Mechanistic Kidney Model to Predict Renal Clearance. *CPT Pharmacometrics Syst Pharmacol* **7**:593–602.

Ismail M, Lee VH, Chow CR, and Rubino CM (2018) Minimal Physiologically Based Pharmacokinetic

and Drug-Drug-Disease Interaction Model of Rivaroxaban and Verapamil in Healthy and Renally Impaired Subjects. *J Clin Pharmacol* **58**:541–548.

Jamei M (2016) Recent Advances in Development and Application of Physiologically-Based Pharmacokinetic (PBPK) Models: a Transition from Academic Curiosity to Regulatory Acceptance, Current Pharmacology Reports.

Jamei M, Dickinson GL, and Rostami-Hodjegan A (2009) A framework for assessing inter-individual variability in pharmacokinetics using virtual human populations and integrating general knowledge of physical chemistry, biology, anatomy, physiology and genetics: A tale of "bottom-up" vs "top-down" recognition of covariates. *Drug Metab Pharmacokinet* **24**:53–75.

January CT, Wann LS, Alpert JS, Calkins H, Cigarroa JE, Conti JB, Ellinor PT, Ezekowitz MD, Field ME, Murray KT, Sacco RL, Stevenson WG, Tchou PJ, Tracy CM, Yancy CW, Members F, Anderson JL, Halperin JL, Albert NM, Bozkurt B, Brindis RG, Creager MA, Curtis LH, Demets D, Guyton RA, Hochman JS, Kovacs RJ, Ohman EM, Pressler SJ, Sellke FW, Shen W-K, Stevenson WG, and Yancy CW (2014) 2014 AHA/ACC/HRS Guideline for the Management of Patients With Atrial Fibrillation. *J Am Coll Cardiol* **63**:e1–e76.

Kubitza D, Becka M, Voith B, Zuehlsdorf M, and Wensing G (2005) Safety, pharmacodynamics, and pharmacokinetics of single doses of BAY 59-7939, an oral, direct factor Xa inhibitor. *Clin Pharmacol Ther* **78**:412–421.

Kubitza D, Becka M, Wensing G, Voith B, and Zuehlsdorf M (2005) Safety, pharmacodynamics, and pharmacokinetics of BAY 59-7939 - An oral, direct Factor Xa inhibitor - After multiple dosing in healthy male subjects. *Eur J Clin Pharmacol* **61**:873–880.

Lumen AA, Li L, Li J, Ahmed Z, Meng Z, Owen A, Ellens H, Hidalgo IJ, and Bentz J (2013) Transport Inhibition of Digoxin Using Several Common P-gp Expressing Cell Lines Is Not Necessarily Reporting Only on Inhibitor Binding to P-gp. *PLoS One* **8**:e69394.

Menochet K, Kenworthy KE, Houston JB, and Galetin A (2012) Simultaneous Assessment of Uptake and Metabolism in Rat Hepatocytes: A Comprehensive Mechanistic Model. *J Pharmacol Exp Ther* **341**:2–15.

Moore KT, Vaidyanathan S, Natarajan J, Ariyawansa J, Haskell L, and Turner KC (2014) An open-label study to estimate the effect of steady-state erythromycin on the pharmacokinetics, pharmacodynamics, and safety of a single dose of rivaroxaban in subjects with renal impairment and normal renal function. *J Clin Pharmacol* **54**:1407–1420.

Mueck W, Kubitza D, and Becka M (2013) Co-administration of rivaroxaban with drugs that share its

elimination pathways: pharmacokinetic effects in healthy subjects. *Br J Clin Pharmacol* **76**:455–466.

Mueck W, Stampfuss J, Kubitza D, and Becka M (2014) Clinical pharmacokinetic and pharmacodynamic profile of rivaroxaban. *Clin Pharmacokinet* **53**:1–16.

Naud J, Michaud J, and Beauchemin S (2011) Effects of chronic renal failure on kidney drug transporters and cytochrome P450 in rats. *Drug Metab Dispos* **39**:1363–1369.

Neely M (2017) Scalpels not hammers: The way forward for precision drug prescription. *Clin Pharmacol Ther* **101**:368–372.

Orr STM, Ripp SL, Ballard TE, Henderson JL, Scott DO, Obach RS, Sun H, and Kalgutkar AS (2012) Mechanism-based inactivation (MBI) of cytochrome P450 enzymes: Structure-activity relationships and discovery strategies to mitigate drug-drug interaction risks. *J Med Chem* **55**:4896–4933.

Prasad B, Johnson K, Billington S, Lee C, Chung GW, Brown CDA, Kelly EJ, Himmelfarb J, and Unadkat JD (2016) Abundance of Drug Transporters in the Human Kidney Cortex as Quantified by Quantitative Targeted Proteomics. *Drug Metab Dispos* **44**:1920–1924.

Rodgers T, and Rowland M (2006) Physiologically based pharmacokinetic modelling 2: Predicting the tissue distribution of acids, very weak bases, neutrals and zwitterions. *J Pharm Sci* **95**:1238–1257.

Rostami-Hodjegan A (2018) Reverse Translation in PBPK and QSP: Going Backwards in Order to Go Forward With Confidence. *Clin Pharmacol Ther* **103**:224–232.

Sager JE, Yu J, Ragueneau-Majlessi I, and Isoherranen N (2015) Physiologically Based Pharmacokinetic (PBPK) Modeling and Simulation Approaches: A Systematic Review of Published Models, Applications, and Model Verification. *Drug Metab Dispos* **43**:1823–37.

Scaglione F (2013) New Oral Anticoagulants: Comparative Pharmacology with Vitamin K Antagonists. *Clin Pharmacokinet* **52**:69–82.

Scotcher D, Jones CR, Galetin A, and Rostami-Hodjegan A (2017) Delineating the Role of Various Factors in Renal Disposition of Digoxin through Application of Physiologically Based Kidney Model to Renal Impairment Populations. *J Pharmacol Exp Ther* **360**:484–495.

Shebley M, Fu W, Badri P, Bow D, and Fischer V (2017) Physiologically Based Pharmacokinetic Modeling Suggests Limited Drug-Drug Interaction Between Clopidogrel and Dasabuvir. *Clin Pharmacol Ther* **102**:679–687.

Shebley M, Sandhu P, Emami Riedmaier A, Jamei M, Narayanan R, Patel A, Peters SA, Reddy VP, Zheng M, de Zwart L, Beneton M, Bouzom F, Chen J, Chen Y, Cleary Y, Collins C, Dickinson GL, Djebli N, Einolf HJ, Gardner I, Huth F, Kazmi F, Khalil F, Lin J, Odinecs A, Patel C, Rong H, Schuck E, Sharma P, Wu SP, Xu Y, Yamazaki S, Yoshida K, and Rowland M (2018) Physiologically Based Pharmacokinetic Model Qualification and Reporting Procedures for Regulatory Submissions: A Consortium Perspective. *Clin Pharmacol Ther*, doi: 10.1002/cpt.1013.

Stampfuss J, Kubitza D, Becka M, and Mueck W (2013) The effect of food on the absorption and pharmacokinetics of rivaroxaban. *Int J Clin Pharmacol Ther* **51**:549–561.

Takács-Novák K, Szoke V, Völgyi G, Horváth P, Ambrus R, and Szabó-Révész P (2013) Biorelevant solubility of poorly soluble drugs: Rivaroxaban, furosemide, papaverine and niflumic acid. *J Pharm Biomed Anal* **83**:279–285.

Tsuruya Y, Nakanishi T, Komori H, Wang X, Ishiguro N, Kito T, Ikukawa K, Kishimoto W, Ito S, Schaefer O, Ebner T, Yamamura N, Kusuhara H, and Tamai I (2017) Different Involvement of OAT in Renal Disposition of Oral Anticoagulants Rivaroxaban, Dabigatran, and Apixaban. *J Pharm Sci* **106**:2524–2534.

US FDA (2017) Drug Development and Drug Interactions : Table of Substrates , Inhibitors and Inducers, Center for Drug Evaluation and Research.

US FDA (2011a) XARELTO (rivaroxaban). Clinical Pharmacology and Biopharmaceutics Review.

US FDA (2011b) XARELTO (rivaroxaban) product information.

Vermeer LMM, Isringhausen CD, Ogilvie BW, and Buckley DB (2016) Evaluation of Ketoconazole and Its Alternative Clinical CYP3A4/5 Inhibitors as Inhibitors of Drug Transporters: The In Vitro Effects of Ketoconazole, Ritonavir, Clarithromycin, and Itraconazole on 13 Clinically-Relevant Drug Transporters. *Drug Metab Dispos* **44**:453–459.

Wang J, and Flanagan DR (1999) General solution for diffusion- controlled dissolution of spherical particles. 1. Theory. *J Pharm Sci* **88**:731–738.

Wessler JD, Grip LT, Mendell J, and Giugliano RP (2013) The P-glycoprotein transport system and cardiovascular drugs.

Wise DL (2000) *Handbook of Pharmaceutical Controlled Release Technology*, CRC Press.

Xu R, Ge W, and Jiang Q (2018) Application of physiologically based pharmacokinetic modeling to the prediction of drug-drug and drug-disease interactions for rivaroxaban. *Eur J Clin Pharmacol* **74**:755–765, European Journal of Clinical Pharmacology.

Zhao X, Sun P, Zhou Y, Liu Y, Zhang Huilin, Mueck W, Kubitza D, Bauer RJ, Zhang Hong, and Cui Y (2009) Safety, pharmacokinetics and pharmacodynamics of single/multiple doses of the oral, direct Factor Xa inhibitor rivaroxaban in healthy Chinese subjects. *Br J Clin Pharmacol* **68**:77–88.

FOOTNOTES

This work was supported by the Singapore Ministry of Education Tier 1 Academic Research Funding to E.C.Y.C. [Grant R-148-000-193-112], the National University of Singapore (NUS) President's Graduate Fellowship (PGF) to E.J.Y.C. and the NUS, Department of Pharmacy, Final Year Project Funding to D.W.X.T. and D.X.Y.C. [Grant C-148-000-003-001]. The authors thank Dr. Kathleen Giacomini (University of California, San Francisco, CA) for the kind donation of the hOAT1-transfected and hOAT3-transfected HEK cell lines.

LEGENDS FOR FIGURES

Figure 1. PBPK modeling framework detailing the iterative processes of model development and verification that were performed in this study. Successful model verification must precede application of the PBPK model of rivaroxaban for prospective predictions of drug-drug-disease interactions.

Figure 2. Simulated pharmacokinetic profiles of rivaroxaban after single dose administration. Simulated mean (solid line) plasma drug concentration-time profiles of single dose rivaroxaban demonstrated (**A**) the effect of food in increasing bioavailability at the 20 mg dose and accurately recapitulated clinically observed profiles at (**B**) 10 mg and (**C**) 20 mg doses. Open symbols represent clinical data.

Figure 3. *In vitro* investigation of the P-gp-mediated and OAT3-mediated transport kinetics of rivaroxaban. For efflux kinetics, time-and concentration-dependent data in the absorptive direction was analyzed via mechanistic three-compartmental modeling. Goodness of fit between experimentally measured (symbols) and simulated (solid lines) basolateral rivaroxaban concentrations is presented in (**A**) and (**B**). For uptake kinetics, time-and concentration-dependent rivaroxaban uptake into OAT3-transfected HEK cells was analyzed via mechanistic two-compartmental modeling. Goodness of fit between experimentally measured (symbols) and simulated (solid lines) intracellular rivaroxaban concentrations is presented in (**C**) and (**D**).

Figure 4. Development of the mechanistic kidney model (MechKiM) for simulation of rivaroxaban PK in healthy and renal impaired patients. Simulated (**A**) cumulative urinary excretion of rivaroxaban and (**B**) its corresponding plasma concentration-time profile using MechKiM following a single 20 mg dose. Accounting for glomerular filtration (black solid line), glomerular filtration and reabsorption (grey dashed line), glomerular filtration, reabsorption and apical P-gp-mediated active efflux (blue dotted line) as well as glomerular filtration, reabsorption and basolateral OAT3-mediated uptake (red line) were unsuccessful in recapitulating observed clinical profiles (open circles). Recapitulation of observed

clinical plasma rivaroxaban concentrations and urinary excretion data required the consideration of basolateral uptake in tandem with apical efflux (orange line). Upon verification of the drug-dependent parameters within the MechKiM model, adjustment of system parameters (glomerular filtration and proximal tubular cells per gram kidney) allowed accurate prediction of the increase in rivaroxaban's systemic exposure in (**C**) mild renal impairment. Open symbols represent clinical data.

Figure 5. Simulated pharmacokinetic profiles of verapamil and its major metabolite norverapamil. Simulated plasma concentration-time profiles of (**A**) 80 mg immediate release verapamil and norverapamil in healthy volunteers verified the basal PBPK model of verapamil provided within Simcyp. (**B**) IVIVC convolution using the reported *in vitro* dissolution profile of a controlled release capsule was unable to recapitulate clinically observed plasma concentration-time profiles following a single 120 mg dose. Iterative refinement of dissolution parameters yielded an *in vivo* dissolution profile (**B**) that adequately described absorption kinetics after (**C**) single and (**D**) multiple dosing based on the administration schedule delineated by Greenblatt *et al.* Open symbols represent clinical data while solid lines depict simulations.

Figure 6. Predicted drug-drug interactions (DDIs) between rivaroxaban and verapamil or ketoconazole in healthy and renal impaired patients. Simulated mean plasma concentration-time profiles of (**A**) 20 mg rivaroxaban in the absence and presence of CYP3A4 inhibitor verapamil demonstrated accurate estimation of DDI magnitude, including (**B**) an increase in the cumulative urinary excretion of rivaroxaban with verapamil co-administration. (**C**) Mild renal impairment potentiated the extent of DDI between rivaroxaban and verapamil. (**D**) Consideration of the inhibitory potential of ketoconazole on CYP3A4/2J2-mediated metabolism and P-gp-mediated efflux of rivaroxaban underestimated the observed DDI magnitude (blue solid line). Optimization of the K_i of ketoconazole against OAT3-mediated rivaroxaban uptake was required to accurately recapitulate the clinically observed DDI (blue dashed line). Open symbols represent clinical data.

DMD Fast Forward. Published on September 10, 2019 as DOI: 10.1124/dmd.119.086918
This article has not been copyedited and formatted. The final version may differ from this version.

Table 1. Key input parameters for the PBPK model of rivaroxaban

Parameter	**Value**	**Method/Reference**
Molecular weight (g/mol)	435.88	CAS ID: 366789-02-8
log P	1.5	(Mueck *et al.*, 2014)
Compound type	Neutral	-
B/P	0.71	(Grillo *et al.*, 2012)
fu	0.065	(Grillo *et al.*, 2012)
Main plasma binding protein	Human serum albumin	-
Absorption Model	ADAM Model	
fu_{gut}	0.21	Predicted
$P_{eff,man}$ (10^{-4}cm/s)	3.020492	Predicted
Permeability Assay	Caco-2	(Gnoth *et al.*, 2011)
Apical pH : Basolateral pH	7.4 : 7.4	
Activity	Passive & Active	
$P_{appA:B}$(10^{-6} cm/s)	8	
Reference Compound	Multiple	
Reference Compound $P_{appaA:B}$ (10^{-6} cm/s)	0	
Scalar	1.284077	Predicted
Solubility pH Type	Intrinsic	
Solubility (mg/mL)	0.01	(Takács-Novák *et al.*, 2013)
Transporter	ABCB1 (P-gp/MDR1)	
J_{max} (pmol/min)	37.83	Determined experimentally
K_m (μM)	9.416	Determined experimentally
fu_{inc}	1	Predicted
Insert growth area of the Transwell (cm^2)	0.33	Determined experimentally
System	MDCK	Determined experimentally
RAF/REF	1.5	
Distribution Model	Full PBPK Model	

V_{SS} (L/kg)	0.3824139	Predicted - Method 2
Enzyme	CYP3A4	Predicted in Simcyp using the Retrograde Calculator
Pathway	Pathway 1	
CL_{int} (µL/min/pmol)	0.06353705	
Enzyme	CYP2J2	Predicted in Simcyp using the Retrograde Calculator
Pathway	Pathway 1	
CL_{int} (µL/min/pmol)	5.685421	
CL_{int} (HLM) (µL/min/mg protein)	7.998799	Predicted in Simcyp using the Retrograde Calculator
Mechanistic Kidney Model		
$CL_{PD,basal}$ (mL/min/million proximal tubular cells)	1.09E-05	Determined experimentally
$CL_{PD,apical}$ (mL/min/million proximal tubular cells)	1.09E-05	Determined experimentally
$fu_{kidney,cell}$	0.3788975	Predicted in Simcyp
fu_{urine}	1	
Transporter	SLC22A8 (OAT3)	
Function	Uptake	
$CL_{int,T}$ (µL/min/million cells)	43	Scaled using sensitivity analysis
Transporter	ABCB1 (P-gp/MDR1)	
Function	Efflux	
J_{max} (pmol/min/million cells)	80.921	Determined experimentally
K_m (µM)	9.416	Determined experimentally
RAF/REF	4	

B/P, blood to plasma partition ratio; CL_{int}, *in vitro* intrinsic clearance; $CL_{int,T}$, *in vitro* transporter-mediated intrinsic clearance; CL_{PD}, passive diffusion clearance; CL_R, renal clearance; fm (liver), fractional metabolism in the liver; f_u, fraction unbound in plasma; fu_{gut}, fraction unbound in the enterocytes; fu_{inc}, fraction unbound in the *in vitro* incubation; $fu_{kidney,cell}$, fraction unbound in the kidney cell; fu_{inc}, fraction unbound in the urine; J_{max}, maximum rate of transporter mediated efflux or uptake; K_m, Michaelis constant; K_p, tissue to plasma partition

DMD Fast Forward. Published on September 10, 2019 as DOI: 10.1124/dmd.119.086918
This article has not been copyedited and formatted. The final version may differ from this version.

coefficient; log P, common logarithm of the octanol:water partition coefficient; MDCK, Madin Darby Canine Kidney cell line; P_{eff}, Human jejunum effective permeability; RAF/REF, Relative activity/expression factor; V_{ss}, volume of distribution at steady state

Table 2. Comparison of PK parameters between simulated and observed data for model verification of rivaroxaban in healthy subjects

	Simulated (n=220)		**Observed (n=22)**	
20 mg single dose, fasted (Stampfuss *et al.*, 2013)	**AUC (µg.h/L)**	**C_{max} (µg/L)**	**AUC (µg.h/L)**	**C_{max} (µg/L)**
Geometric mean	1512	111	1477	160
CV (%)	67	28	23	34
Ratio of simulated/observed	1.02	0.69		
Success criteria for ratio of simulated/observed	0.81-1.23	0.74-1.35		

	Simulated (n=220)		**Observed (n=22)**	
20 mg single dose, fed (Stampfuss *et al.*, 2013)	**AUC (µg.h/L)**	**C_{max} (µg/L)**	**AUC (µg.h/L)**	**C_{max} (µg/L)**
Geometric mean	2127	234	2048	281
CV (%)	31	28	23	27
Ratio of simulated/observed	1.04	0.83		
Success criteria for ratio of simulated/observed	0.81-1.23	0.79-1.27		

	Simulated (n=200)			**Observed (n=20)**		
10 mg single dose (Mueck *et al.*, 2013)	**AUC (µg.h/L)**	**C_{max} (µg/L)**	**CL (L/h)**	**AUC (µg.h/L)**	**C_{max} (µg/L)**	**CL (L/h)**
Geometric mean	1103	139	9.06	892	138	11.20
CV (%)	31	24	41	27	22	27
Ratio of simulated/observed	1.24	1.01	0.81			
Success criteria for ratio of simulated/observed	0.78-1.29	0.81-1.23	0.78 - 1.29			

DMD Fast Forward. Published on September 10, 2019 as DOI: 10.1124/dmd.119.086918
This article has not been copyedited and formatted. The final version may differ from this version.

	Simulated (n=130)			Observed (n=13)		
20 mg single dose (Greenblatt *et al.*, 2018)	**AUC (µg.h/L)**	**C_{max} (µg/L)**	**CL (L/h)**	**AUC (µg.h/L)**	**C_{max} (µg/L)**	**CL (L/h)**
Geometric mean	2685	266	7.45	2583	263	7.92
CV (%)	40	29	49	21	26	23
Ratio of simulated/observed	1.04	1.01	0.94			
Success criteria for ratio of simulated/observed	0.78 - 1.29	0.74- 1.35	0.76 - 1.31			

AUC, area under the concentration-time curve from time zero to infinity; C_{max}, maximum plasma concentration; CV, coefficient of variation

DMD Fast Forward. Published on September 10, 2019 as DOI: 10.1124/dmd.119.086918
This article has not been copyedited and formatted. The final version may differ from this version.

Table 3. J_{max} and K_m of P-gp-mediated efflux activity, and passive permeability (P_{pass}) of rivaroxaban in MDCK-MDR1 cell monolayers derived from three compartmental analysis

		Absorptive Transport	
	***In vitro* data** **(initial estimates)**	***Nelder-Mead***	***Hybrid***
J_{max} (pmol/min)	97.98 [a]	37.83 (24.3, 51.4)	41.63 (26.2, 57.1)
K_m (µM)	836.80 [a]	9.42 (7.0, 11.8)	12.36 (8.9, 15.8)
$P_{pass} \times 10^{-6}$(cm/s)	6.37 [b]	12.88 (9.8, 15.9)	12.48 (9.5, 15.4)
R^2	-	0.97	0.97
AIC	-	49.80	59.47
AIC_c	-	50.82	60.40
		Uptake Transport	
$CL_{int,T}$ (µL/min/10^6 cells)	33.91	41.33 (40.18, 42.47)	-
CL_{PD} [c] (µL/min/10^6 cells)	1.09×10^{-5} (Fixed)		
R^2		0.97	-
AIC		-16.92	-
AIC_c		-16.44	-

Confidence intervals (95%) are described in brackets.

[a] $J_{max,app}$ and $K_{m,app}$ derived from conventional Michaelis Menten analysis and $CL_{int,T}$ estimate derived from conventional two step approach (**Supplemental Fig. 2**).

[b] P_{pass} determined from inhibition of P_{app} measured in the absorptive direction in the presence of 100 µM of verapamil.

[c] Fixed using CL_{PD} estimated from P_{pass} of 12.88 × 10-6 cm/s using **eq. 3** as large standard errors have been observed with CL_{PD} estimated using 2 min incubations (Menochet *et al.*, 2012).

DMD Fast Forward. Published on September 10, 2019 as DOI: 10.1124/dmd.119.086918
This article has not been copyedited and formatted. The final version may differ from this version.

Table 4. Comparison of PK parameters between simulated and observed data for model verification of the mechanistic kidney model in both healthy and renal impaired patients

	Simulated (n=130)			**Observed (n=13)**		
20 mg single dose, Healthy[a], P-gp Only (Greenblatt *et al.*, 2018)	**AUC (µg.h/L)**	**C_{max} (µg/L)**	**CL_R (L/h)**	**AUC (µg.h/L)**	**C_{max} (µg/L)**	**CL_R (L/h)**
Geometric mean	3901	311	0.37	2583	263	2.42
CV (%)	52	31	27	21	26	23
Ratio of simulated/observed	***1.51***	1.18	***0.15***			
Success criteria for ratio of simulated/observed	0.78 - 1.29	0.74- 1.35	0.76 - 1.31			
	Simulated (n=130)			**Observed (n=13)**		
20 mg single dose, Healthy[a], OAT3 Only (Greenblatt *et al.*, 2018)	**AUC (µg.h/L)**	**C_{max} (µg/L)**	**CL_R (L/h)**	**AUC (µg.h/L)**	**C_{max} (µg/L)**	**CL_R (L/h)**
Geometric mean	2946	269	1.60	2583	263	2.42
CV (%)	45	30	46	21	26	23
Ratio of simulated/observed	1.14	1.02	***0.66***			
Success criteria for ratio of simulated/observed	0.78 - 1.29	0.74- 1.35	0.76 - 1.31			
	Simulated (n=130)			**Observed (n=13)**		
20 mg single dose, Healthy[a], P-gp and OAT3 (Greenblatt *et al.*, 2018)	**AUC (µg.h/L)**	**C_{max} (µg/L)**	**CL_R (L/h)**	**AUC (µg.h/L)**	**C_{max} (µg/L)**	**CL_R (L/h)**
Geometric mean	2563	263	2.70	2583	263	2.42
CV (%)	43	30	49	21	26	23

Ratio of simulated/observed	0.99	1	1.12			
Success criteria for ratio of simulated/observed	0.78 - 1.29	0.74- 1.35	0.76 - 1.31			
	Simulated (n=200)			**Observed (n=20)**		
10 mg single dose, Healthy[a], P-gp and OAT3 (Mueck *et al.*, 2013)	**AUC (µg.h/L)**	**C_{max} (µg/L)**	**CL_R (L/h)**	**AUC (µg.h/L)**	**C_{max} (µg/L)**	**CL_R (L/h)**
Geometric mean	1060	120	3.05	892	138	2.5
CV (%)	40	29	55	27	22	26
Ratio of simulated/observed	1.19	0.87	1.22			
Success criteria for ratio of simulated/observed	0.78- 1.29	0.81- 1.23	0.78- 1.28			
	Simulated (n=140)			**Observed (n=14)**		
20 mg single dose, Mild Renal Impairment[b] (Greenblatt *et al.*, 2018)	**AUC (µg.h/L)**	**C_{max} (µg/L)**	**CL_R (L/h)**	**AUC (µg.h/L)**	**C_{max} (µg/L)**	**CL_R (L/h)**
Geometric mean	2899	279	1.46	2864	252	2.25
CV (%)	43	29	50	29	29	42
Ratio of simulated/observed	1.01	1.11	0.65			
Success criteria for ratio of simulated/observed	0.72- 1.38	0.72- 1.38	0.63- 1.58			
Fold Change vs Healthy[c]	**AUC Fold Change (90% CI)**		**CL_R Fold Change (90% CI)**	**AUC Fold Change**		**CL_R Fold Change**
	1.20 (1.09, 1.31)		0.54 (0.49, 0.60)	1.11		0.93
Success Criteria for Fold Change	0.80-1.81		0.30-1.03			

DMD Fast Forward. Published on September 10, 2019 as DOI: 10.1124/dmd.119.086918
This article has not been copyedited and formatted. The final version may differ from this version.

AUC, area under the concentration-time curve from time zero to infinity; C_{max}, maximum plasma concentration; CL_R, renal clearance; CV, coefficient of variation
[a]Healthy controls (CrCL > 80mL/min)
[b]Mild Renal Impairment (defined as CrCL: 50-79 mL/min)
[c]PK parameters in healthy controls utilized for comparison were obtained from simulations where the mechanistic kidney model incorporating both P-gp and OAT-3 was used to simulate the plasma concentration-time profile of rivaroxaban after a single 20 mg dose

DMD Fast Forward. Published on September 10, 2019 as DOI: 10.1124/dmd.119.086918
This article has not been copyedited and formatted. The final version may differ from this version.

Table 5. Summary of CYP450 and P-gp inhibition parameters with rivaroxaban as probe substrate

***In Vitro* Parameters**		**Verapamil**	**Norverapamil**	**Ketoconazole**
MBI of CYP3A4	K_I **(µM)**	1.65	0.28	-
	K_{inact} **(h^{-1})**	3.92	2.44	-
	K_{inact}/K_I **($\mu M^{-1} h^{-1}$)**	2.38	8.59	-
Reversible Inhibition of CYP3A4	**Mode**	Mixed	Mixed	Mixed
	K_i **(µM)**	0.487	0.270	0.094
	α	1.19	1.15	3.28
Reversible Inhibition of CYP2J2	**Mode**	Competitive	Competitive	Competitive
	K_i **(µM)**	12.2	162	0.082
	α	-	-	-
	R_1[a]	1.00	1.00	
Fraction Unbound in the *In Vitro* Incubation	fu_{inc}	0.67	0.78	1
Inhibition of P-gp	IC_{50} **(µM)**	4.3[b]	-	0.22
Inhibition of OAT3	IC_{50} **(µM)**			

[a]R_1 is the predicted ratio of the victim drug's area under the plasma concentration-time curve in the presence and absence of an inhibitor for basic models of reversible inhibition. $R_1 = 1 + (I_{max,u}/K_i)$ where $I_{max,u}$ is the maximal unbound plasma concentration of the interacting drug.
[b]IC_{50} value of verapamil on the P-gp-mediated efflux of rivaroxaban (1 µM) across L-MDR1 cells after 2 h incubation at 37°C (Gnoth *et al.*, 2011)

DMD Fast Forward. Published on September 10, 2019 as DOI: 10.1124/dmd.119.086918
This article has not been copyedited and formatted. The final version may differ from this version.

Table 6. Simulated change in rivaroxaban PK parameters in the presence of drug-drug or drug-drug-disease interactions

	Simulated (n=100)			Observed (n=10)		
Rivaroxaban 20 mg and Verapamil (Greenblatt *et al.*, 2018)	**AUC (µg.h/L)**	**C_{max} (µg/L)**	**CL (L/h)**	**AUC (µg.h/L)**	**C_{max} (µg/L)**	**CL (L/h)**
Geometric mean	3488	314	5.73	3600	278	5.70
CV (%)	43	28	56	20	27	22
Ratio of simulated/observed	0.97	1.13	1.01			
Success criteria for ratio of simulated/observed	0.77-1.31	0.70-1.43	0.75-1.34			
Fold Change vs Healthy[a]	**AUC Fold Change (90% CI)**		**CL Fold Change (90% CI)**	**AUC Fold Change**		**CL Fold Change**
	1.46 (1.33, 1.61)		0.68 (0.62, 0.75)	1.39		0.72
Success Criteria for Fold Change	0.94- 2.05		0.45–1.04			
	Simulated (n=110)			**Observed (n=11)**		
Rivaroxaban 20 mg and Verapamil in Mild Renal Impairment[b] (Greenblatt *et al.*, 2018)	**AUC (µg.h/L)**	**C_{max} (µg/L)**	**CL (L/h)**	**AUC (µg.h/L)**	**C_{max} (µg/L)**	**CL (L/h)**
Geometric mean	4057	327	4.93	4093	267	5.04
CV (%)	41	27	73	29	29	26

Ratio of simulated/observed	0.99	1.22	0.98					
Success criteria for ratio of simulated/observed	0.69-1.44	0.60-1.44	0.72-1.39					
Fold Change vs Healthy	**AUC Fold Change (90% CI)**		**CL Fold Change (90% CI)**		**AUC Fold Change**		**CL Fold Change**	
	1.70 (1.54, 1.87)		0.59 (0.53, 0.65)		1.58		0.64	
Success Criteria for Fold Change	0.97-2.57		0.40-1.01					
	Simulated (n=200)				**Observed (n=20)**			
Rivaroxaban 10 mg and Ketoconazole (Mueck *et al.*, 2013)	**AUC (µg.h/L)**	**C_{max} (µg/L)**	**CL_H (L/h)**	**CL_R (L/h)**	**AUC (µg.h/L)**	**C_{max} (µg/L)**	**CL_H[c] (L/h)**	**CL_R (L/h)**
Geometric mean	1676	189	2.66	3.05	2298	237	2.75	1.60
CV (%)	39	23	38	54	26	20	26	33
Ratio of simulated/observed	***0.73***	***0.80***	0.97	***1.91***				
Success criteria for ratio of simulated/observed	0.78-1.28	0.83-1.21	0.78-1.28	0.74-1.36				
Fold Change vs Healthy	**AUC Fold Change (90% CI)**	**CL_H Fold Change (90% CI)**	**CL_R Fold Change (90% CI)**		**AUC Fold Change**	**CL_H Fold Change**	**CL_R Fold Change**	
	1.56 (1.46 , 1.66)	0.45 (0.42, 0.49)	1.01 (0.92, 1.09)		2.58	0.32	0.64	
Success Criteria for Fold Change	1.48-4.50	0.17-0.58	0.38–1.07					
	Simulated (n=200)				**Observed (n=20)**			

DMD Fast Forward. Published on September 10, 2019 as DOI: 10.1124/dmd.119.086918
This article has not been copyedited and formatted. The final version may differ from this version.

Rivaroxaban 10 mg and Ketoconazole **OAT3 K_i Optimized** **(Mueck *et al.*, 2013)**	**AUC (µg.h/L)**	**C_{max} (µg/L)**	**CL_H (L/h)**	**CL_R (L/h)**	**AUC (µg.h/L)**	**C_{max} (µg/L)**	**CL_H[c] (L/h)**	**CL_R (L/h)**
Geometric mean	2850	241	2.70	0.81	2298	237	2.75	1.60
CV (%)	35	21	36	30	26	20	26	33
Ratio of simulated/observed	1.24	1.02	0.98	***0.51***				
Success criteria for ratio of simulated/observed	0.78-1.28	0.83-1.21	0.78-1.28	0.74-1.36				

Fold Change vs Healthy	**AUC Fold Change (90% CI)**	**CL_H Fold Change (90% CI)**	**CL_R Fold Change (90% CI)**	**AUC Fold Change**	**CL_H Fold Change**	**CL_R Fold Change**
	2.65 (2.49, 2.82)	0.44 (0.41, 0.48)	0.27 (0.25, 0.29)	2.58	0.32	0.64
Success Criteria for Fold Change	1.48-4.50	0.17-0.58	0.38–1.07			

AUC, area under the concentration-time curve from time zero to infinity; CL, clearance; CL_H, hepatic clearance, CL_R, renal clearance; C_{max}, maximum plasma concentration; CV, coefficient of variation

[a]PK parameters in healthy controls utilized for comparison were obtained from simulations where the mechanistic kidney model incorporating both P-gp and OAT-3 was used to simulate the plasma concentration-time profile of rivaroxaban after a single 10 mg or 20 mg dose (**Table 3**).

[b]Mild Renal Impairment (defined as CrCL: 50-79 mL/min).

[c]CL_H calculated from ($CL/F - CL_R$) assuming F=1 as rivaroxaban is known to have high absolute bioavailability (80-100%) for the 10 mg dose (Mueck *et al.*, 2013).

DMD Fast Forward. Published on September 10, 2019 as DOI: 10.1124/dmd.119.086918
This article has not been copyedited and formatted. The final version may differ from this version.

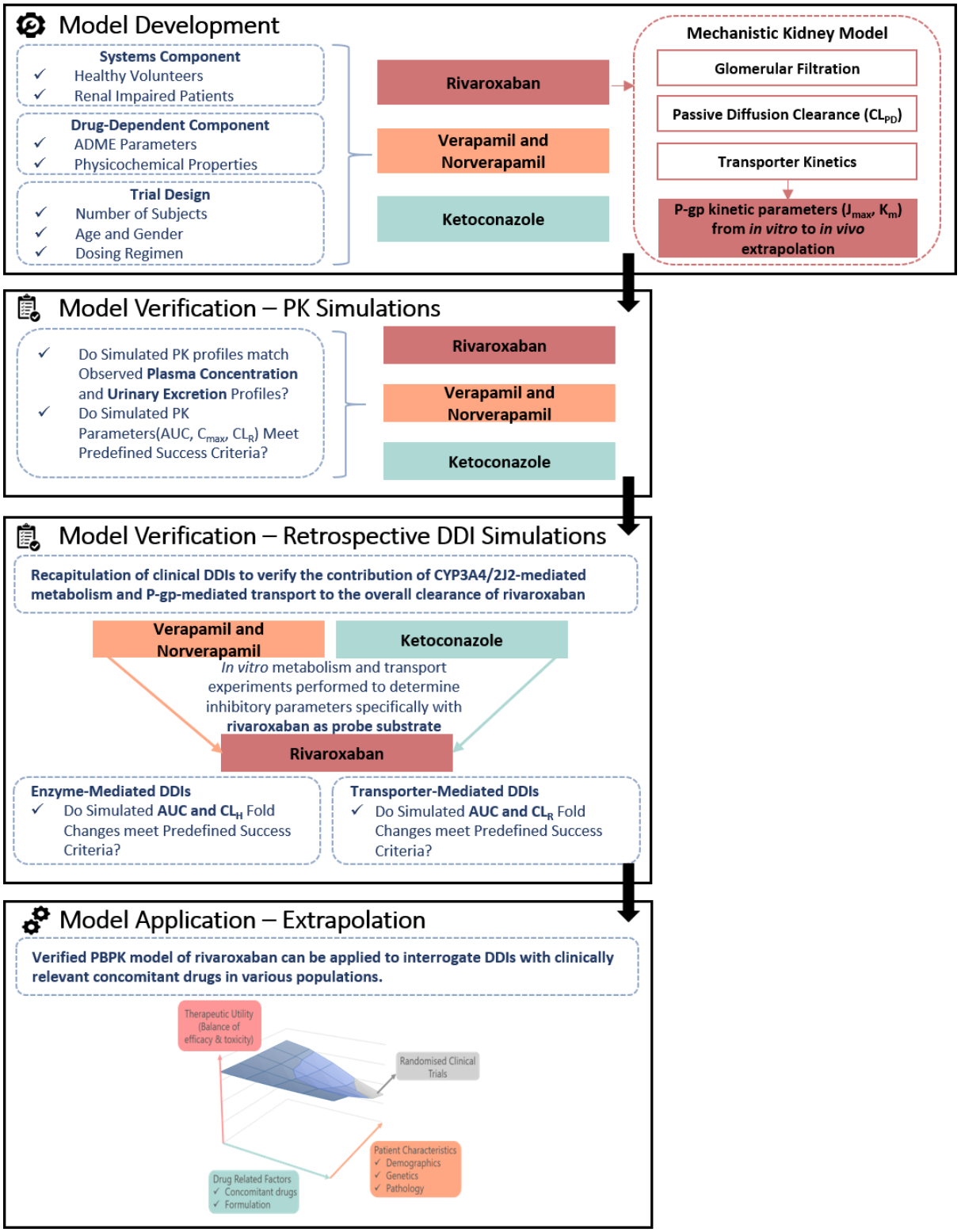

Figure 1

DMD Fast Forward. Published on September 10, 2019 as DOI: 10.1124/dmd.119.086918
This article has not been copyedited and formatted. The final version may differ from this version.

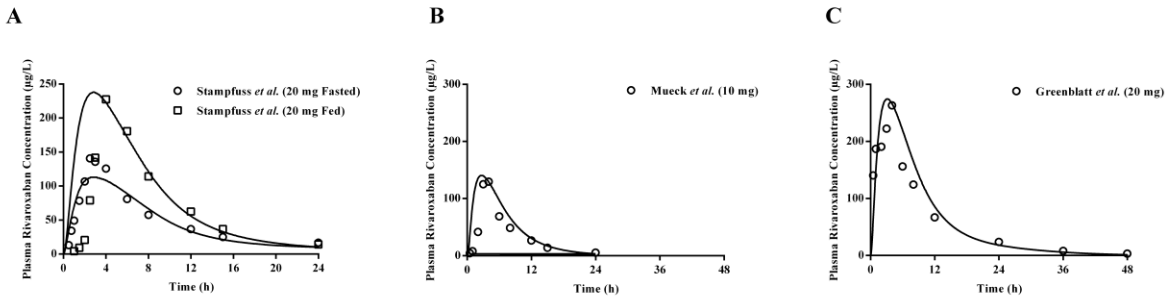

Figure 2

DMD Fast Forward. Published on September 10, 2019 as DOI: 10.1124/dmd.119.086918
This article has not been copyedited and formatted. The final version may differ from this version.

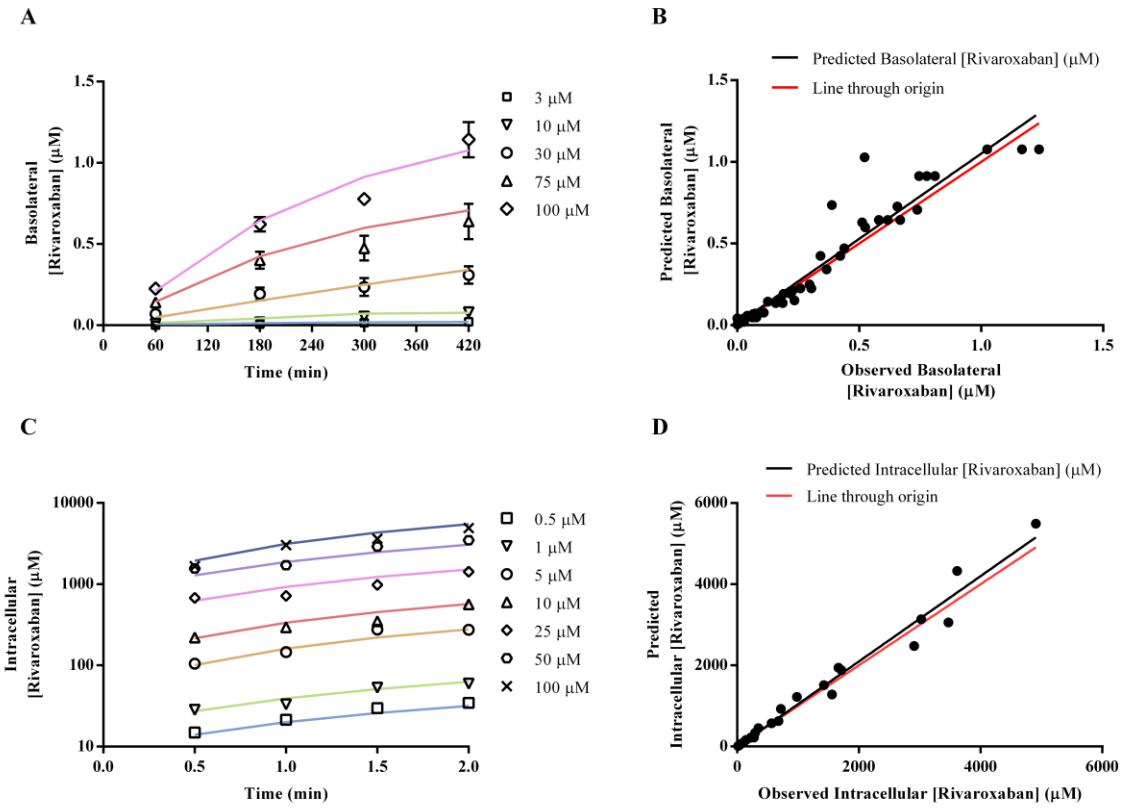

Figure 3

DMD Fast Forward. Published on September 10, 2019 as DOI: 10.1124/dmd.119.086918
This article has not been copyedited and formatted. The final version may differ from this version.

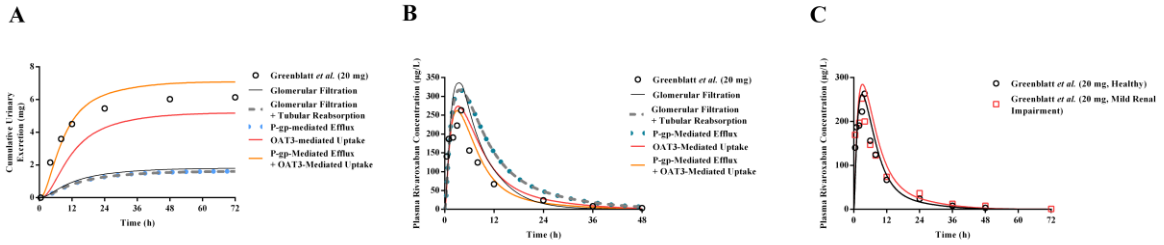

Figure 4

DMD Fast Forward. Published on September 10, 2019 as DOI: 10.1124/dmd.119.086918
This article has not been copyedited and formatted. The final version may differ from this version.

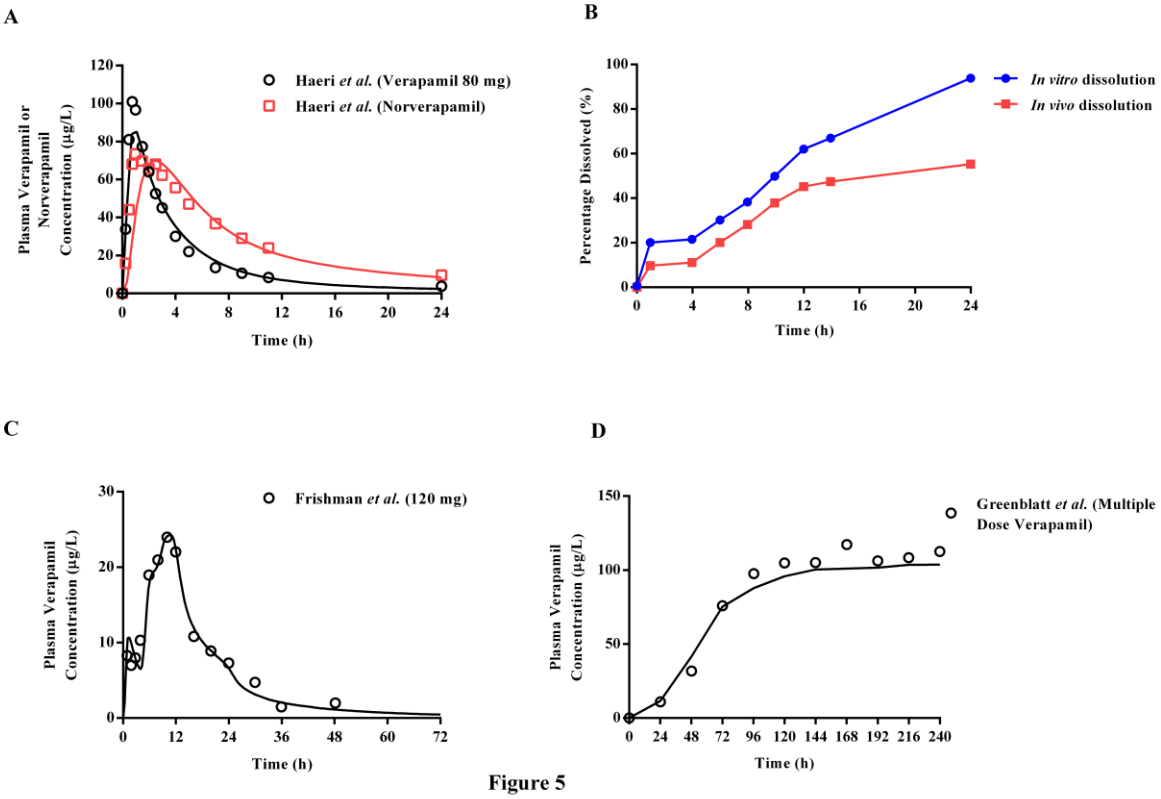

Figure 5

DMD Fast Forward. Published on September 10, 2019 as DOI: 10.1124/dmd.119.086918
This article has not been copyedited and formatted. The final version may differ from this version.

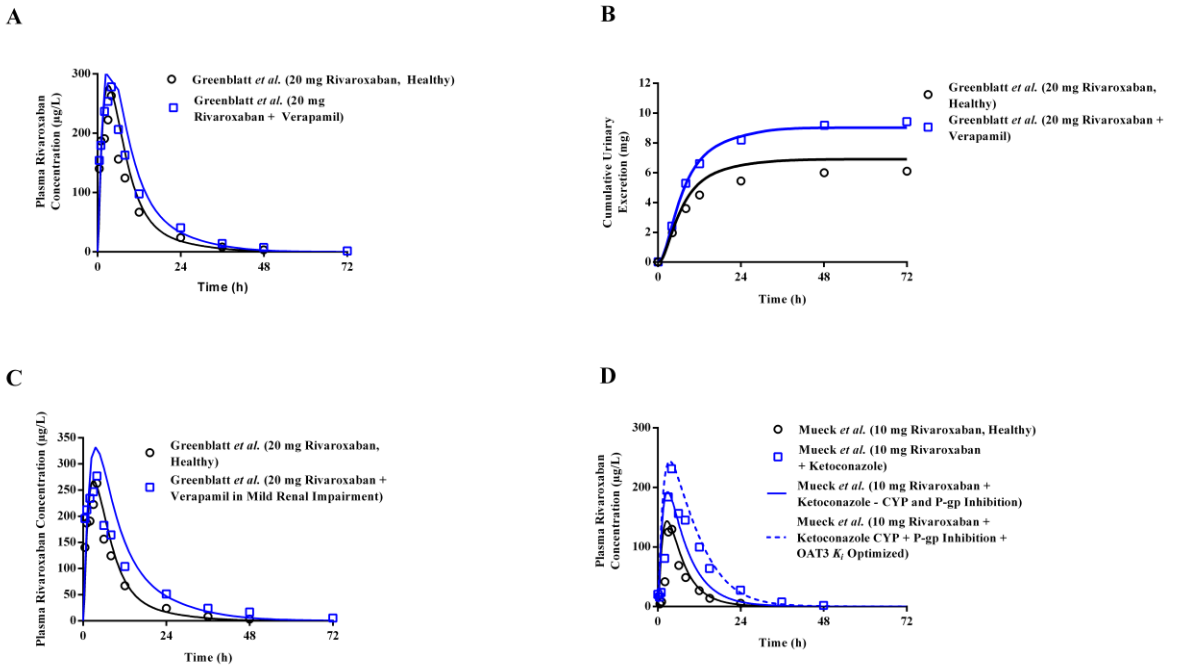

Figure 6